Development of Analytical & Optimization Tools for Double-Acting Hydrogen Direct Injection Technology

by

Martin Geh
Bachelor in Engineering, University of Victoria, 2003

A Thesis Submitted in Partial Fulfillment
of the Requirements for the Degree of

MASTERS OF APPLIED SCIENCE

in the Department of Mechanical Engineering

Supervisory Committee

Development of Analytical & Optimization Tools for Double Acting Hydrogen Direct Injection Technology

by

Martin Geh
Bachelor in Engineering, University of Victoria, 2003

Supervisory Committee

Dr. A. Rowe, (Department of Mechanical Engineering)
Supervisor

Dr. S. Dost, (Department of Mechanical Engineering)
Co-Supervisor or Departmental Member

Dr. J. Provan, (Department of Mechanical Engineering)
Departmental Member

Abstract

Supervisory Committee
Dr. A. Rowe, (Department of Mechanical Engineering)
Supervisor
Dr. S. Dost, (Department of Mechanical Engineering)
Co-Supervisor or Departmental Member
Dr. J. Provan, (Department of Mechanical Engineering)
Departmental Member

One of the market leaders in hydrogen injection systems for internal combustion engines has developed double acting direct injection technology for a wide range of fuel pressures. This thesis outlines the development and validation of a solenoid model which predicts static magnetic forces as well as the development of a dynamic lift model which predicts injector motion and impact forces. The solenoid force model found that iron cobalt can be replaced by iron silicon materials as there performance is comparable. The dynamic lift model shows that the seat and stop impact forces can be calculated which allows engineers to optimize injector designs before prototypes are built. These models allow engineers to optimize the performance and geometric parameters of the double acting technology in preparation of series production.

Table of Contents

List of Tables

List of Figures

Nomenclature

NOx	-	Nitrogen Oxides (typically NO, NO_2)
PFI	-	Ported Fuel Injection
DI	-	Direct Injection
ICE	-	Internal Combustion Engine
SQUID	-	Superconducting Quantum Interference Device
CO_2	-	Carbon dioxide
HC	-	Unburned Hydrocarbon
CNG	-	Compressed Natural Gas
DA	-	Double Acting
DAI	-	Double Acting Injector
PPS	-	Polyphenelyne Sulfide
PWM	-	Pulse Width Modulated

Symbols

V_1/V_2	Compression ratio	H	Magnetic Field Strength
T_1, T_2	absolute initial, final temperature	μ	Permeability of surrounding media
γ	Ratio of specific heats	H_d	Demagnetising Field
i	Coil current	N_d	Geometric Factor
δl	Elemental length of a conductor	M	Magnetisation
r	Radial distance from conductor	H_{in}	Corrected Magnetic Field Strength
u	Unit vector along radial direction	H_{app}	Applied Magnetic Field Strength
δH	Magnetic field at r due to current iδl	B	Magnetic Induction (A/m)
N	Number of current-carrying conductors	μ_o	Permeability of Free Space
r_a	Average conductor radius	Mo	Magnetic Moment
μ_r	Material Relative Permeability	V	Sample Volume
h_C	Height of Coil	Φ_{coil}	Coil Current Density
w_C	Width of Coil	M_1	Upper Injector Needle Mass
M_2	Lower Injector Needle Mass	x_1	Upper Needle Mass Displacement
x_2	Lower Needle Mass Displacement	F_U	Upper Magnetic Force
F_L	Lower Magnetic Force	d_t	Stop Damping Coefficient
k_t	Stop Spring Constant	d_r	Connecting Rod Damping Coefficient
k_r	Connecting Rod Spring Constant	k_s	Return Spring Spring Constant
k_p	Seat spring Constant	d_p	Seat damping coefficient
F_p	Internal Injector Pressure Force	F_{pre}	Return Spring Preload
F_{f1}	Upper Guide Friction Force	F_{f2}	Lower Guide Friction Force

$\ddot{x}_1, \ddot{x}_2$	Upper & Lower Needle Mass Acceleration	$\dot{x}_1, \dot{x}_2$	Upper & Lower Needle Mass Velocity
F_{Rseat}	Seat Reaction Force	F_{Rstop}	Stop Reaction Force
g	Gravity	H_{max}	Maximum Injector Lift
F_c	Coulomb Friction Force	F_{brk}	Break Away Friction Force
F_s	Stribeck Friction Force	Fv	Viscous Friction Force
v	Velocity	C_v	Friction coefficient
f_v	Viscous friction coefficient	V_{th}	Velocity Threshold
A_e	Effective Area	P_i	Internal Injector Pressure
P_o	Downstream Injector Pressure		

Acknowledgments

I would like thank Dr. Andrew Rowe, my supervisor for supporting this work with his knowledge and guidance which made this project possible. I also thank my managers Dr. Peter Steinrück and Dr. Gerhard Ranegger, for providing not only the means but also the support required to complete a project of this magnitude. I also thank Dr. Matthias Opel and the Walther-Meißner-Institute for all the magnetic material measurements performed. Finally I would like to thank my wife and family for supporting me and this project.

Chapter 1 Introduction

1.1 Motivation

Increasing fuel prices and worries about global warming have heightened interest from governments, consumers, and automobile manufactures in alternative fuels and alternatives to the common internal combustion engine. The recent success of hybrid powered vehicles in the US market proves that consumers are becoming more aware of fuel prices and are willing to invest in alternatives to the standard internal combustion engine [1].

Although vehicle manufacturers are taking steps toward cleaner, more fuel efficient vehicles such as ultra-clean diesel engines or hybrid systems, the fact remains that, due to the ever dwindling reservoirs, fossil fuels are not the fuel of the future. Currently, vehicle manufactures and governments are spending billions of dollars on the development of hydrogen fuel cells to power electric cars [2]. Unfortunately, automakers estimate this technology's commercialization feasibility will not occur before 2015, because industry still needs to overcome challenges such as hydrogen distribution, durability, power density, freeze start characteristics and production costs [3]. Many automakers, such as BMW and Ford, acknowledge that the hydrogen economy is coming and so have begun developing a stepping-stone technology to bridge the gap until the fuel cell is ready for the consumer market. This technology is the hydrogen powered internal combustion engine which has the advantage of using the already highly developed internal combustion engine (ICE) while producing near-zero carbon dioxide and reduced NOx vehicle emissions. The technology does have some hurdles to overcome. These include the availability of hydrogen suitable for fuel and a complete lack of a distribution network. But, as a transition technology, it showcases what the hydrogen economy will be like and allows people to become used to the idea of hydrogen as a fuel. The hydrogen ICE is currently a viable solution for fleet and public transportation applications which provides a market and therefore an incentive for fuel company's to build production and distribution networks. This initial investment in distribution networks would then allow for large scale introduction of fuel cell powered vehicles.

There are also engine specific challenges which must be overcome before the hydrogen ICE becomes viable, which include: on-vehicle storage, re-fueling, and injection technology. Hydrogen injection technology has been a research topic of interest in the automotive industry beginning with ported fuel injection and now direct injection (DI) technology. Initial designs of DI technology were limited due to needle bounce, high cylinder combustion pressure/temperature, slow closing times and constrained fuel pressure range.

Injector bounce occurs when the injector needle impacts the seat while closing and is characterized as uncontrolled movement of the injector needle after the initial injector closure. The bouncing of the needle allows additional fuel into the combustion process resulting in unstable cycle to cycle combustion. Figure 1-1 shows a typical lift profile of a high pressure injector. The top curve shows the lift of the injector needle obtained using a reflective light distance measuring technique while the bottom curve shows the current flowing through the solenoid. The bouncing of the needle can be seen after 5ms when the current is no longer flowing and the needle lift shows a sinusoidal decaying motion.

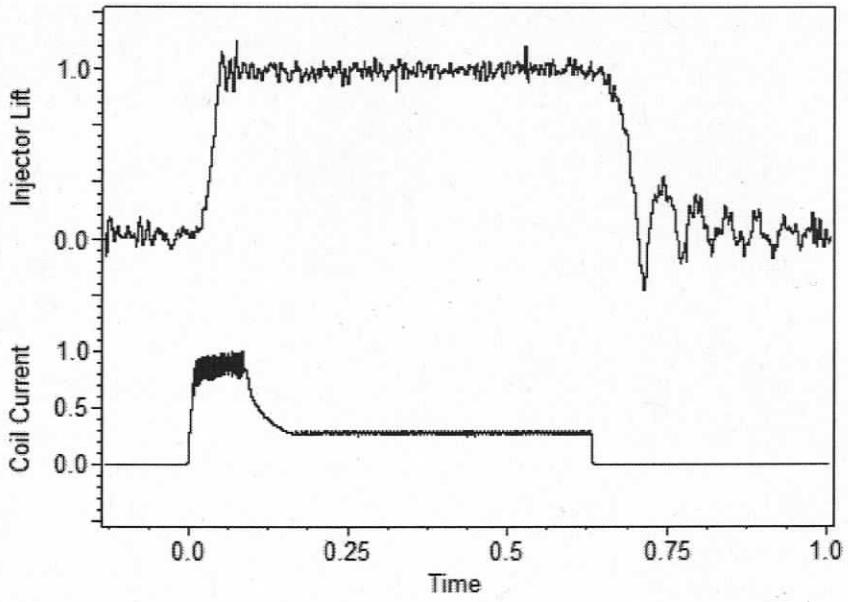

Figure 1-1: Measured high pressure injector lift showing needle bounce.

In previous development work needle lift and inlet pressure were shown to have little

influence on the bouncing of the injector needle while changes in the seat or needle materials and closing spring force had a large influence on the amplitude as well as the rate of damping. A solution to reduce needle bounce implemented a composite needle design. The injector needle comprised of a steel body with an injection moulded plastic needle shaft which due to its length absorbed much of the impact energy. This reduced the bouncing to acceptable levels.

An increase in closing spring force also showed promise, but due to geometric constraints as well as injector opening dynamics this option could not be perused. The introduction of the injection moulded plastic needle reduced injector needle wear due to reduced weight and therefore lower impact forces. It had the negative effect that the maximum allowable seat temperature became critical, the needle material softened and permanent damage occurred at temperatures above 120℃ which is within the normal operating range for a hydrogen ICE.

Another problem encountered by first generation injectors was that fuel pressure was limited to high pressures (100-300bar) since the required flow area need for hydrogen presents a large needle surface for the combustion pressure to act on. To balance this force and to ensure the injector remains closed during combustion, the high fuel pressure acts together with the return spring. Increasing the return spring force to compensate for lower fuel pressure is not effective in decreasing minimum fuel pressure. The flow area requirements increase with lower fuel pressure and so the force acting during combustion increases making the required return spring geometry unfeasible. The only method for developing a low pressure DI injector (0-100 bar) involved changing the injector concept from an inwards opening to an outwards opening injector which presents technical challenges in both injector design and engine operation which still must be overcome.

The successful operation of high pressure injectors increased interest in middle pressure (20 – 80 bar) fuel injection. Low pressure injection has the disadvantage in terms of combustion efficiency due to reduced injection energy which enables charge mixing. It does have the advantage that it effectively uses current hydrogen gas storage pressures to

increase vehicle range. The difficulty in designing a low pressure direct injector comes from the pressure difference between the fuel and cylinder. The low fuel pressure requires a larger injector flow rate which is achieved at the cost of an increase in the area which the combustion pressure can act. For example, in high pressure injectors, the fuel pressure of 200 bars applies a force on the needle which is larger than the force that can be applied by the combustion pressure, and, hence, the return spring force can be small. In the case of a low pressure injector, the force applied by the fuel pressure is smaller than the force resulting from the combustion pressure, and so the spring force must be large to keep the injector closed during combustion. The problem arises in that the required spring force becomes larger than the available opening magnetic force thus resulting in an injector which does not open.

As a solution to this problem, a double acting (DA) gaseous fuel injector concept which eliminated and/or reduced the limiting factors has been developed. This enabled a wide range of fuel and combustion pressure with opening and closing speed comparable to that of modern liquid direct injection systems. This technology has shown promise in a wide range of hydrogen engine applications. However, there are still many challenges to overcome before the technology can be applied to series production vehicles. The main challenges faced are: installation geometry, durability, cost, and ballistic/multiple injection capability.

1.2 Objectives

This thesis describes the development of a set of modeling tools which allow engineers to optimize the design of DA DI injectors for hydrogen ICE's. The main challenges to be solved, before this technology can be used in production vehicles includes reducing the installation geometry, increasing durability, increasing performance and reducing production and material costs. The solution to these challenges involves the optimization of the magnetic circuit in terms of material, and required performance, as well as analysis of the impact forces which, through optimization of materials, coatings, and geometry, can reduce the seat and stop wear, fulfilling the automotive life time requirements of 5000 hours of operation.

The analysis of the magnetic circuit involves the creation of a finite element model which will be validated using the current combination of materials and geometry used in the prototype injectors. The model will be validated based on the comparison of measured and simulated static forces which simulate the opening and closing conditions of the magnetic circuit used in DA injectors. Using the validated model a range of alternative materials will be analyzed to determine the relationship between performance, magnetic core diameter and material cost.

The surface-to-surface impact between the needle and seat or stop in DA injectors causes unacceptable wear rates and, in hydrogen applications, failure of protective coatings. A model of injector dynamics is used to predict impact forces thereby allowing for better selection of materials and coatings as well as impact surface size to reduce injector needle and seat/stop wear. The model will also allow for predication of opening and closing times based on return spring forces, magnetic forces and component masses.

Chapter 2 Direct Injection Technology

The modern internal combustion engine is a complex system of mechanical components, electronic controllers, sensors, and chemical reactions The systems work together to optimize performance and fuel consumption while also regulating emissions output to below legislated levels. The air-fuel ratio is one of the primary engine parameters which defines power output and emissions at a given load. The methods of introducing the required fuel to produce the air-fuel ratio within an engine can be divided into three categories: carbureted, port side fuel injection and DI. Carbureted fuel injection involves centrally mixing the air and fuel before it enters the engine manifold. This method is no longer employed in the automotive industry due to the inherently poor air fuel ratio control and the resulting high emissions. Port side fuel injection involves injection of the fuel within the air manifold just before each cylinder intake valve. As the name implies, DI involves injecting the fuel directly into the cylinder. DI is considered a state-of-the-art technology in the automotive industry because the precise fuel control reduces emissions, increases cylinder power output, and increases engine fuel economy.

The following discussion will give an overview of the current automotive liquid DI systems used for both diesel and gasoline engines. It will be explained why this technology cannot be used in gaseous applications as well as what design considerations must be fulfilled by a gaseous DI system for the operation of a hydrogen ICE. The discussion will then provide an overview of the current state of gaseous injection technology as well as the application of this technology to hydrogen IC engines.

2.1 Liquid Fuel Direct Injection Systems

Direct injection of fuel into an ICE requires precise control over combustion related parameters such as air-fuel ratio, injection timing, fuel pressure and intake/exhaust valve timing. The complexity of the system is justified by the increase in cylinder power output, reduced fuel consumption, and in combination with exhaust after treatment low emissions. This method of mixture formation has the advantage that the maximum cylinder volume can be filled with air, and once the intake valve is closed, the fuel is

injected resulting in a high cylinder fill rate which increases the power output. This method is used exclusively in diesel engines and is just starting to be adapted to Otto cycle engines. The main disadvantage of this method is the short time available for mixing. To solve this problem, DI systems inject fuel at high pressure (~2000 bar) which leads to fine droplet formation as the fuel passes through the nozzle. It is important that the spray angle and droplet size are correct otherwise the mixture will be inhomogeneous, resulting in engine knock or high emissions.

There are three factors which make DI technology more complex than that of external mixture formation. These factors are (1) cylinder pressure and temperature, (2) short injection times and (3) vaporization of fuel.

As the name implies fuel injectors for DI technology are exposed to the conditions in the cylinder throughout the combustion cycle. The cylinder pressure can reach 130 bars during combustion which requires that injectors be designed to resist opening during these periods otherwise back flow of combustion gases will occur. The injector tip- including the nozzle, seat and needle are exposed to changing temperatures related to the combustion and intake/exhaust phases. These temperature spikes can lead to thermal expansion or warping of sealing surfaces if the injector design does not include thermal expansion compensation and good surface connections to cylinder head cooling channels.

A fuel injector used for DI applications must react and complete the injection within only a few milliseconds during the compression stroke of the engine. This requirement places a high demand on the actuation system as well as the seat and needle sealing surfaces. Depending on the engine concept, multiple injections may also be needed to achieve layered fuel mixtures or to induce cylinder swirl which enables low emissions or high power output.

Due to the short time available for both injection and mixing, the injectors must inject a fine droplet spray of fuel into the cylinder which vaporizes and mixes quickly with the compressed air. Today the most efficient method of creating the fine droplet spays is by

forcing the fuel under high pressure through a nozzle equipped with fine holes. The hole sizes are in the range of only a few hundredths of a millimeter and must be precision machined and hydro-ground to eliminate any burs which could alter the flow pattern [4]. The high pressure required to generate the spray is in the range of 2000 to 3000 bar [4]. The high pressures required for injection are usually generated directly in the injector (a single unit system) or by an external high pressure pump integrated into the injection system (a common rail system).

Figure 2-1 shows a typical single unit system where the high pressure required for DI is generated in the injector. The system is made up of three main components: fuel compressor, injection needle and control valve. The fuel compressor is activated by a cam shaft which begins to compress the fuel under the piston. The growing pressure forces the valve needle to open and injection begins. To control the close timing of the injector, the control valve opens dropping the pressure drops which in turn closes the injector. Common rail injection systems operate on the same principal except that the pressure in constantly applied thus keeping the injector closed during the high pressure combustion phase.

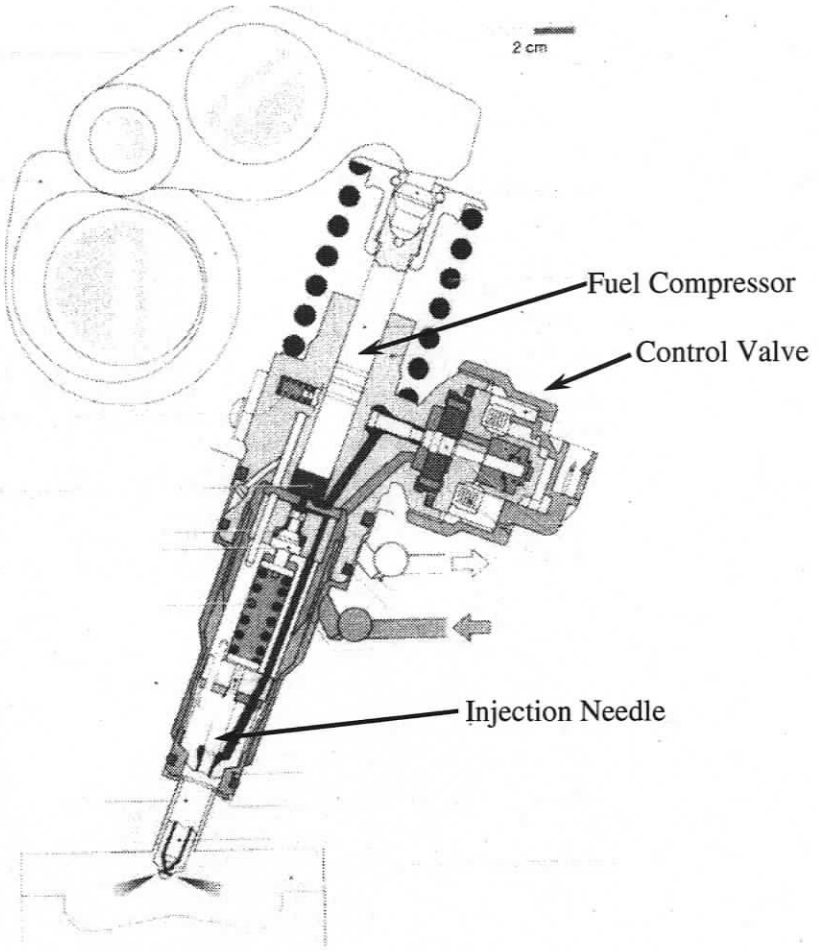

Figure 2-1: Typical direct injector for a single unit system [4].

The basic design concept of using the fuel as hydraulic fluid to open and close the injector through the means of a control valve has not changed since the initial conception of DI systems. There are however two components which have been intensely studied and optimized, namely control valve and seat/needle/nozzle geometry.

The control valve determines the opening and closing of the injector by controlling when and for how long the pressure is allowed to act on the needle. The fuel, acting as a hydraulic fluid, is virtually incompressible which means the reaction speed of the needle is directly related to the speed of the control valve [4]. In the past, control valves have been electromechanically actuated using fast switching solenoids which provide opening and closing speeds high enough to allow up to 4 injections per injection cycle [4]. The

greater the number of injections per cycle, the better the control of the mixture formation which allows for improved control over the combustion process. This has led systems designers to design piezo-actuated control valves. These piezo-actuated valves use a piezoelectric stack instead of a solenoid to control the injector needle motion. The advantage of the piezoelectric stack is that it reacts quickly and its stroke is proportional to the voltage applied. This technology allows for between 8 and 10 injections per cycle as well as step-less injection profiles [4].

The second area of optimization is the seat/needle/nozzle geometry. Direct injectors are designed so that the nozzle and seat are one component thereby reducing the dead volume in the nozzle. Dead nozzle volume includes all the volume after the seal including spay holes where fuel remains open to combustion in liquid form. This fuel cannot be burned effectively and is a source of unburned hydrocarbon (HC) emissions. The seat and needle are designed based on a conical seal design as shown by the examples in Figure 2-2 which also shows various dead volume designs.

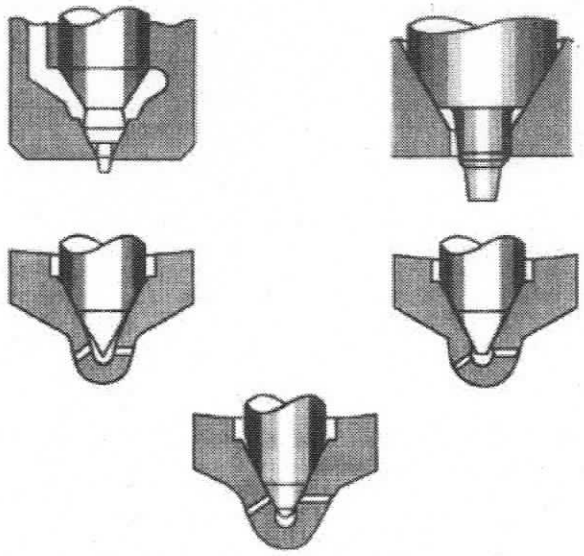

Figure 2-2: Typical nozzle/seat/needle designs [4]

Liquid DI technology based on the usage of the fuel as a hydraulic fluid as described above is considered state of the art in the automobile industry. There are, however, projects and working examples of fuel injectors which use piezo or magnetostrictive

technology to directly actuate the needle. This has the advantage of eliminating the last bit of lag caused by the compressibility of the fuel. However, this technology is plagued by thermal expansion problems due to the long stack or rod lengths required to produce the specified needle stroke. This problem has been addressed using hydraulic or mechanical thermal compensators, which add an additional level of complexity to the design. [4]

2.2 Gaseous DI Design Considerations

DI of gaseous fuels such as natural gas and hydrogen is currently an area of interest in the automotive industry due to low fuel costs and reduced emissions. The problem is that unlike fuel injectors for external mixture formation, the current state of art DI technology cannot be applied as the fuel is compressible and thus cannot be used to actuate the needle. Solutions to this problem include the use of directly actuated systems or duel fuel systems where small amounts of liquid fuel aid in opening the valve which is then injected into the cylinder. Once open, a second actuator opens the main valve and the gas begins to fill the cylinder. This system is difficult to apply to the passenger vehicle market due to the need to transport two fuels as well as the geometric restraints of the injector, but it has been successfully applied in heavy duty industrial engine applications. The following discussion presents the design considerations of gaseous DI systems in terms of actuation and sealing. Other considerations such as combustion pressure and temperature requirements are considered to be application dependant and similar to those of liquid fuels.

2.2.1 Injector Actuation

The actuation of gaseous fuel injectors is limited to directly actuated designs due to the compressibility of the fuel which does not allow pressure assisted actuation. The selection of a suitable actuation technology can be made based on the following parameters: actuation speed, maximum stoke, attenuation direction, applicable force, power requirements, shape factor, and cost.

The actuation speed determines the opening and closing times of the injector and is dependent on the speed of the control system and in the case of magnetic methods the

material properties. An injector which opens and closes quickly is characterized by steep opening and closing stroke profile flanks as well as a small phase shift between the control signal and lift profile. The phase shift can be caused by materials properties, injector force balance or, in the case of magnetic methods, eddy current losses. The advantage of a fast reacting injector is better control of the combustion cycle and lower cycle to cycle variance.

Due to the reduced energy density of gaseous fuels, injector designs require large flow areas as compared to liquid DI injectors to produce an equivalent air-fuel ratio. The effective injector flow area is a product of the seat geometry and the stroke. The larger the seat flow geometry the smaller the required stroke but at a cost of high opening forces due to fuel pressure. Depending on the application (high or low pressure DI), an actuator capable of small or large strokes is required. Large flow areas expose more needle surface to the combustion pressure, which is typical of low pressure DI. To compensate, injector designs incorporate return springs sufficiently large to hold the injector needle closed during combustion; however, this high return spring force must be overcome during injection.

Most automakers prefer injector designs where the needle is inwardly actuated. This means the actuator must apply a force to pull the injector away from the nozzle when opening. This type of design is preferred because if the injector fails, the needle remains in the closed position which seals the injector; also, broken injector components are unable to enter the cylinder and cause further damage to pistons or intake/exhaust valves. The disadvantage of this type of design is the inherent dead volume between the seat and nozzle outlet which is not present in outwardly opening injectors.

The power requirement of the actuation system is a critical parameter when selecting an actuation system. Actuation methods requiring large amounts of power are capable of high actuation forces, strokes and speeds but this is offset by reduced efficiency of the entire system. An example is the hydraulically actuated gaseous fuel injector which uses an external hydraulic system to operate the injector. This system provides excellent

injector characteristics but the loss in overall efficiency due to the hydraulic pump and extra vehicle weight makes this solution unviable for passenger car applications.

Due to increasingly compact engine designs, the ratio of actuator diameter and length becomes important. If the actuator is of a long, thin form factor, the distance between cylinder and vehicle hood could limit its application. The same goes for a short fat shape factor, as the space between cylinders may not be sufficient. A long injector design also has the potential for thermal expansion problems due to varying temperatures in the engine compartment compared to that of the injector nozzle tip.

Based on the described requirements, three actuation technologies can be applied to directly actuated gaseous DI injectors: electromagnetic, magnetostrictive and piezoelectric. These three methods are commonly found in liquid injection technology and so have shown robustness in automotive applications. The following is short description of each type of actuation method and how they fulfill the requirements for gaseous fuel injection systems.

Electromagnets in their most basic form consist of an iron rod with a wire coil wrapped around its diameter. When a current is passed through the wire, a magnetic field is produced within the steel rod which is then magnetic. In the automotive industry, there are two types of magnetic solenoids commonly found, as shown in Figure 2-3.

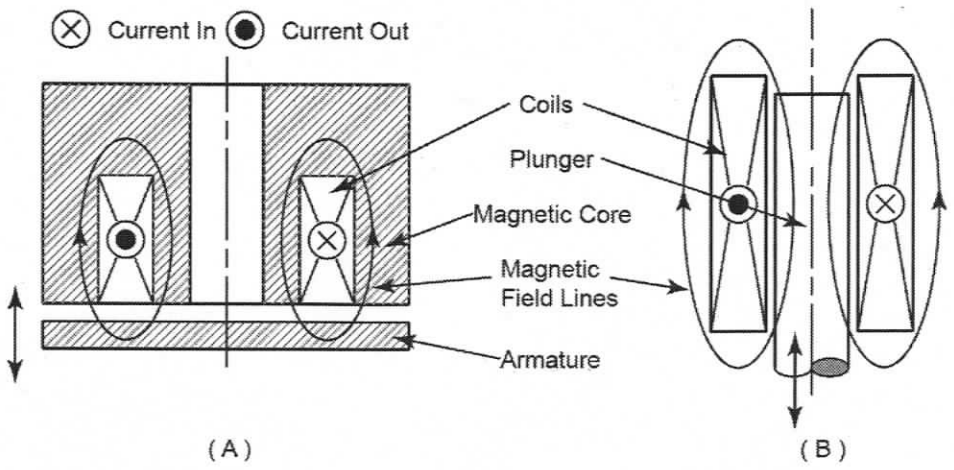

Figure 2-3: Types of solenoid designs.

The solenoid shown in Figure 2-3 (A) consists of a magnetic core and armature manufactured from a soft magnetic material. The magnetic core houses the coil which when energized produces a magnetic field in the core and armature which pulls the armature towards the core. This type of solenoid is characterized as a high force low stroke solenoid. The magnetic force drops exponentially the larger the distance between core and armature, thereby making this type of solenoid only useful in applications where small strokes are required. Solenoids of this type are commonly used as the actuator for liquid DI control valves as shown in Figure 2-1. The solenoid shown in Figure 2-3 (B) consists of a fixed coil which, when energized, produces a magnetic field in a movable plunger. The plunger is then forced out of the coil by the magnetic field. This type of solenoid is capable of producing large stokes with moderate to low forces thereby making it the optimal actuator for ported fuel injectors (liquid and gaseous) due to the low fuel pressure and high flow requirements.

Due to the pressure and flow requirements of hydrogen DI injectors, only the solenoid shown in Figure 2-3 (a) will be further considered as an actuation method. The high force is required to open the injector, while the short stroke can be compensated using multi-ring seat designs in high flow applications. Figure 2-4 shows the response of a typical solenoid as shown in Figure 2-3 (a). As can be seen, the smaller the lift, the greater the force. This shows that any DI injector designed using a solenoid as an actuator must be

sized appropriately to accommodate the desired stroke and force.

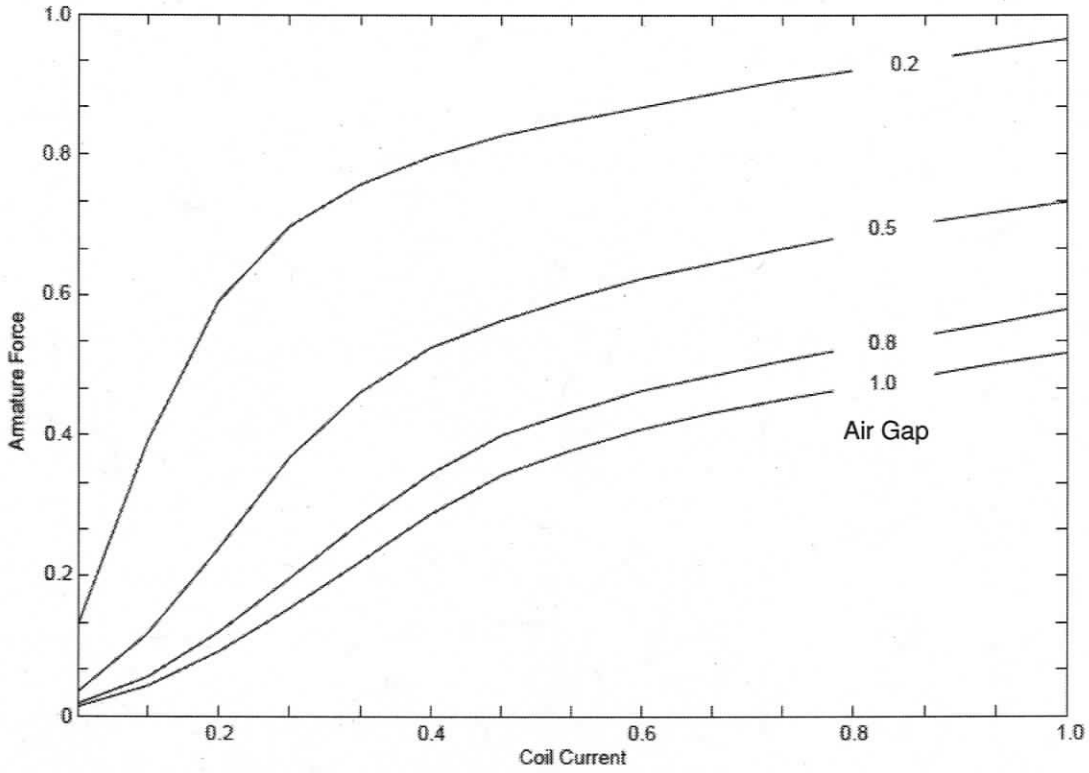

Figure 2-4: Solenoid force curves for various armature distances and coil excitation.

The reaction time of such an actuator is governed by the speed at which the current increases in the coil. As the current increases, the force acting on the armature increases. This means that the booster which produces the peak hold currents used to operate the injector is important. The current begins with a steep climb to a maximum current, which is referred to as peak current. To overcome the impedance of the coil; it is applied with a boost voltage that is typically 45-90V. This initial peak ensures that the maximum force can be quickly generated allowing the injector to open quickly. Once the peak current has been applied, the booster then drops the current to what is called the hold current. This can be done because the gap between the solenoid and armature has been reduced to a rest gap that is typically 0.05 of a millimeter where the solenoid is strongest. This rest gap is present in order to avoid contact between the armature and solenoid thus ensuring that the components are not damaged.

Solenoids do have disadvantages when compared to other actuation technologies, especially when the geometry of the injector is a factor. DI injectors must be designed to fit within the cylinder head of an ICE but, due the complex cooling channel designs and intake/exhaust valve placement, there is often minimal space available to fit the injector. The force generated by the solenoid is restricted by two factors: core diameter and face area, which is limited by the geometric constraints of the cylinder head, and the core material. The net magnetic force between the core and armature can be calculated according to Equation 2.1, where M is the local magnetization of the core and B is the local magnetic flux.

$$\vec{F} = \int \nabla(\vec{M} \cdot \vec{B}) dV \tag{2.1}$$

Thus, the force is determined by the volume of the body, applied field strength and the magnetic permeability of the material. The volume of space for the injector is independent of the actuator and the applied field strength is constrained by acceptable current density through the coil. Thus, the magnetic properties of the solenoid and armature are the areas where a designer has the greatest degree of freedom. Magnetic properties of typical materials used will be discussed in detail in Chapter 3 and Appendix A.

Magnetostrictive actuation technology uses a property of ferromagnetic materials which change shape when subjected to a magnetic field. This phenomenon occurs when the domains or regions of uniform magnetic polarization within the crystalline structure of the material shift and rotate in the presence of a magnetic field [5]. Figure 2-5 shows a typical design for a magnetostrictive actuator. The coil is wrapped around the rod, and when a current is applied, the rod extends. An advantage to this technology is that the amount of extension is proportional to the current traveling through the coil. Using this property, injectors can be designed to operate using variable strokes which improve control over fuel flow during idle operation. The maximum elongation of a magnetostrictive rod is limited to around 1/1000 of the length of the rod [6]. The short stroke, which is produced by this actuation method, makes it suitable for the design of high pressure injectors with small lift requirements. One problem faced by designers

using this technology is the fact that the thermal expansion of the rod is in the same range as the expansion due the magnetic field. This makes thermal control of the injector important; otherwise the injector lift will be a function of the fuel temperature.

Magnetostrictive actuators are currently being used in DI injectors for CNG powered IC engines. Unfortunately the transfer of the technology to hydrogen powered engines has proven to be difficult since the ferromagnetic materials used corroded rapidly when exposed to hydrogen. Currently, there is research that shows that the rods could be protected through the use of special coatings or by separating the hydrogen from the actuator by using a metallic flexible sealing element such as those used in standard pressure transducers.

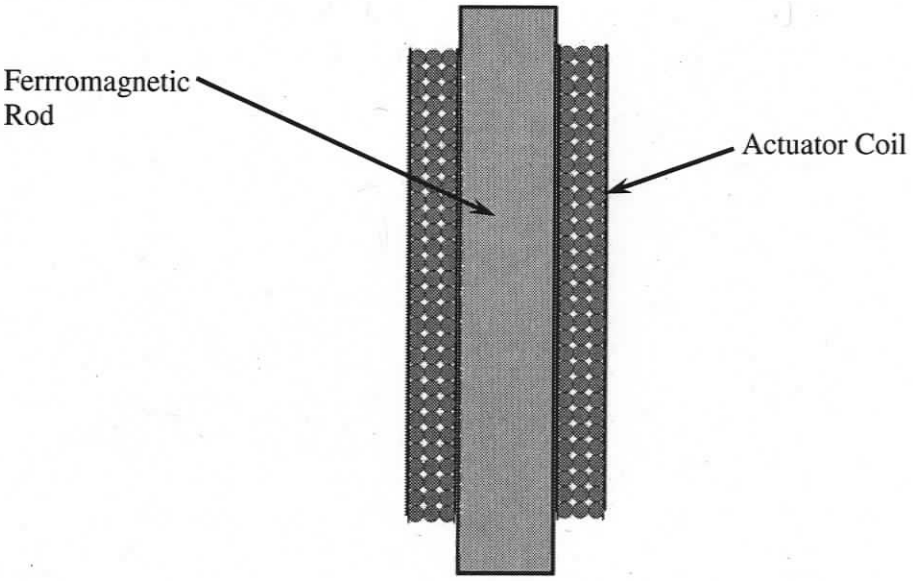

Figure 2-5: Magnetostrictive type actuator.

Piezoelectric actuation technology uses the property of crystalline materials, such as quartz, which expand when subjected to a difference in electrical potential. The effect is similar to that of magnetostrictive actuators except that the movement is initiated using changing potential instead of changing current. A piezo actuator comprises a laminated stack of crystalline material which expands and contracts based the potential applied. A major advantage of the technology is its near instantaneous reaction. This allows for extremely short injection durations and precise control over the injection profile. The

disadvantage of this technology is that in order to achieve the stroke required to provide sufficient flow area, the stack must be long which can be problematic in engine compartment of consumer vehicles. In order to increase the lift, the expansion of the actuator is amplified either through mechanical or hydraulic means, which can introduce a delay in the reaction, but also reduce stack height. The application of piezo technology is hindered in gaseous applications due to the manufacture and development of piezo actuators. This is a specialized field, and it is often difficult to obtain piezo actuator due to the costs involved. These costs are hard to justify in today's small hydrogen injector market. However, this technology does show promise for the future should a large fleet of vehicles use hydrogen as a fuel.

2.2.2 Injector Internal Sealing

The seal between the fuel and combustion chamber is critical to ensuring proper operation of IC engines. During the exhaust phase, the unburned fuel due to injector leakage can cause back fire conditions in the exhaust after treatment system or cause increased emissions. During the intake and compression phase, leaked fuel alters the air-fuel mixture which can cause engine knock and high emissions. Gaseous fuels are difficult to seal as compared to liquid fuels due to the low density and smaller molecular size.

There are two sealing methods used in gaseous fuel injection systems, as shown in Figure 2-6. The sealing systems shown are for inward opening injectors, both methods can also be adapted for outward opening operation.

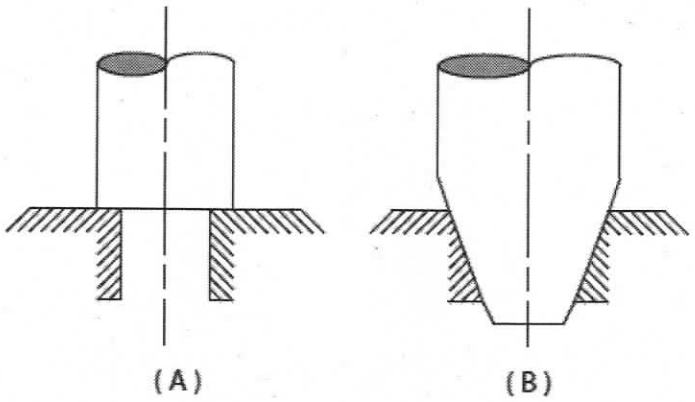

Figure 2-6: Face and conical internal sealing systems.

The sealing method (A) produces the seal using finely machined flat sealing surfaces which are easy to machine. The conical design, as shown by (B), is typical of liquid DI injectors and has proven to be a robust wear free sealing solution. For gaseous applications this seat design is limited due the required surface quality which is difficult to machine as well as the small contact surface (single line of contact) which, due to relative motion in dry atmospheres between the two components, leads to high wear. The single line of contact is also difficult to seal as the conical surface must be exactly conical otherwise the gaps lead to high leakage rates. The conical seat design is also only appropriate for high pressure, low flow applications because, as the seat becomes larger, the pressure forces acting on the needle become large which must be overcome by the actuator. This problem is overcome by the flat sealing method by switching from a hole design to a ring design. See DA injector design details in Section 2.4.3 for more information on ring seal designs.

Special consideration must be taken when designing a seat needle combination for hydrogen applications. The hydrogen flowing through the injector provides no lubrication which protects sealing surfaces from premature wear. Hydrogen also degrades the natural protective coating of hardened steels typically used in seat/needle design which enables conditions for cold welding between the needle and seat. The cold welding caused by contact stress between needle and seat leads to damage and eventual failure of the sealing

surface. Therefore, surfaces subjected to high impact stresses must be coated to eliminate the cold welding under hydrogen atmospheres. The prediction of the impact forces is a main component of this thesis work which will aid in the selection of suitable coatings. For more information see Chapter 4.

2.3 Literature Review Gaseous Injector Design & Modeling

The development and application of injection technology for gaseous ICE applications is a field of interest to automakers and governments because of the emission advantages that gaseous fuels provide. The following literature review will present a short summary of the application of ported gaseous fuel injection technology to hydrogen engines as well as a technology overview of methods used for both CNG and hydrogen DI.

Port injection for CNG applications is an established technology which has been implemented by automakers due to emissions and cost advantages. One such application is the 2008 Honda Civic GX which has a 113hp, 1.4L, 4 cylinder CNG engine. This vehicle is being sold in the US and has a unique fuel feature which allows owners to refuel at home using natural gas used for home heating and cooking. Due to the growth potential of CNG, automotive component companies such as Bosch and Siemens have begun producing fuel injectors specifically designed for CNG. The low energy density of hydrogen limits the use of these injectors for ported fuel injection due to the higher flow rates required per injection. Heffel et al. [7] investigated a series of heavy duty CNG injectors for both variable and constant speed hydrogen IC engines. The results showed that only the largest injector tested was capable of fulfilling the fuelling requirements of the variable speed engine (8.4mg hydrogen in 4.83ms) while all the injectors tested were capable of fuelling the constant speed engine which has applications in hybrid systems. The injectors tested showed good dynamic response and reasonable leakage however no evaluation of long term durability was performed. Kabat et al. [8] performed long term durability testing (64 million injector cycles) on several injector types. The injectors range from standard CNG to modified CNG injectors (Solid lubricant and surface treatment) and prototype injectors designed for hydrogen application. The results were varied, with standard injector designs failing within 75 hours and others reaching the

specified durability target of 800 hours. A subsequent tear down of the injectors showed various failure modes and armature and sealing surface wear.

There have been many attempts to design and validate gaseous DI injectors for both CNG and hydrogen; this section will present a summary of the published injector designs. One company working on DI of gaseous fuel for automotive and heavy duty IC engines is Westport Innovations based in Vancouver Canada. Harrington et al. [9] published the results of a DI heavy-duty diesel engine fuelled using a duel fuel diesel/CNG injection system. The injection system was designed to inject a small pilot amount of diesel followed by the main injection of CNG. The diesel fuel, due its lower auto ignition temperature, produces a pilot flame which ignites the natural gas. The engine tests showed that the engine maintained power characteristics similar to those under diesel operation while providing 40% reduction in NOx and a 71% reduction in particle emissions. Subsequently, Westport has also developed DI CNG and H2 technology which eliminates the need for diesel pilot injection but does require constant glow plug operation to reliably ignite the fuel mixture.

Another approach to gaseous DI is presented by a group of researchers at the University of Concordia, in Montreal, Quebec [10-12]. The injection technology for high pressure gaseous fuels proposed and optimized by the group relies on solenoid direct actuation using a solenoid as shown in Figure 2-3 (B). The injector performance is optimized by using a lumped mass model of the mechanical components as well as a mathematical solenoid model. The optimization efforts produced a control circuit which applied 100 volts to the coil to quickly overcome impedance allowing for switching times comparable to that of fluid DI systems. The initial design was limited due to needle bounce, needle pressure difference and internal leakage. The needle bounce was reduced by incorporating a flexible rod connecting the needle and armature which was designed based on the lumped mass model results. The force balancing and leakage issues were addressed by using a conical seat design with a reversed differential angle which reduced the length of the single contact line between seat and needle. This reduced leakage and allowed for improved force balancing which widened the range of fuel pressure as well as

improved combustion stability during idle operation.

The methods devised for injecting gaseous fuels are numerous. The two methods described above are considered classical injector designs since they rely on technology which is accepted by the automotive industry. Injector designs that use unconventional actuation methods include the vibrating disc [13] and membranes [14], which have yet to be proven in automotive deployment.

2.3.1 Modeling of Gaseous DI injector Dynamics

The modelling of injector dynamics allows for performance prediction and optimization under varying engine conditions. Problems such as needle bouncing can be addressed in the simulation phase of the injector design, thereby reducing the need for design iterations. Liquid fuel DI systems response is dependant on fluid dynamics which, as shown by Mulemane et al. [15], can be accurately modeled using multi-domain software packages like AMEsim which is designed to model electro hydraulic systems. Mulemane uses AMEsim to investigate the dynamic response of a single unit diesel injector. The simulation results were compared to measured data which showed good agreement. However, gaseous fuel injection systems do not rely on fluid dynamical effects for actuation and so the fluid dynamic approach is not suitable to model their response.

Hong et al.[20] presents a method using a lumped-mass spring damper system which is used to optimize a gaseous fuel injector developed by researchers at Concordia University [10 – 12]. The lumped mass method takes into account the gas pressure and solenoid forces which enables the researchers to model the motion of the injector to determine response times and minimize dynamic effects like needle bounce. The model developed by Hong predicts the forces generated by the solenoid using a stored magnetic energy method as shown by Equation 2.2 where h represents the air gap between the solenoid magnetic pole and moving core, Φ the magnetic flux, and W is stored magnetic energy. Equation 2.2 is a simplified solenoid model which assumes steady state response and neglects transient conditions. It should be noted this equation is only valid for plunger type solenoids as shown by Figure 2-3 (B).

$$F_s = -\frac{\partial W(\phi, h)}{\partial h} = -\frac{\phi^2}{2A_l\mu_o} \tag{2.2}$$

Further work by Kekedjian el al. [11] describes the development of a solenoid force model based on experimental results. Measurements were taken which relate the solenoid force to the current in the winding for various air-gaps as well as the solenoid inductance for various air-gaps. Using the collected data a non-linear first order equation was developed which allowed Kekedjian to model both steady state and transient solenoid conditions.

Pohl et al. [21] presents an alternative solenoid force model using a semi-empirical approach. Equations describing a simple inductor and resistor circuit are developed which are then coupled with material hysteresis data. Experimentally determined coil inductance is then used to determine the solenoid force.

The methods published by Pohl, Kekedjian and Hong all use experimentally determined solenoid parameters to develop a solenoid force model. This approach is acceptable when modelling known solenoids as the required parameters can be measured. These models are however difficult to apply when attempting to optimize a solenoid before constructing a prototype.

2.3.2 State of Hydrogen Automotive Industry

The hydrogen power ICE has not yet entered the mainstream automobile market, but several automotive concept projects have been completed which showcase the technology. This section will describe some of the current projects, as well as explaining the application and technology used.

Currently, most hydrogen IC engines rely on ported fuel injection technology. In the automotive sector two companies, BMW and Ford, are considered the industry leaders in the hydrogen ICE industry. BMW began testing and producing the first hydrogen

vehicles in 1984 with the 745i turbo which operated a bivalent engine capable of gasoline or hydrogen combustion. These vehicles were showcased at exhibitions and travelled around the world, proving the technology's reliability, performance and emissions advantages. In 2007, BMW began production of the first series hydrogen car, the BMW Hydrogen 7 which is based on the BMW 7 series sedan. The Hydrogen 7 boasts a 12 cylinder bivalent engine with gasoline DI and hydrogen port side injection. The hydrogen is stored in a liquid form in a cryogenic tank contained in the trunk which is vaporized shortly before reaching the injectors. Ford produced a 10-cylinder, ported hydrogen engine for use in airport shuttle buses. The hydrogen is stored onboard using high pressure storage systems which, due to their size, limit the engine applications to buses. There are also several other smaller projects, such as the development of a hydrogen rotary engine by Mazda.

The current projects for hydrogen DI are limited due to the current state of injection technology. However, there is one project, known as HyFLEET:CUTE, which is currently deploying hydrogen DI technology in buses for the Berlin public transportation system. This project is funded by the European Commission's 6^{th} framework research program and it plans the expansion of the bus fleet to 10 cities worldwide.

2.4 Double Acting Injector Technology

Standard Injector designs have one downward facing solenoid which applies a force on the armature to open the injector. Once current stops flowing within the solenoid the return spring pushes the injector back into the closed position. The DA technology is characterized by the addition of a second solenoid as shown in Figure 2-7.

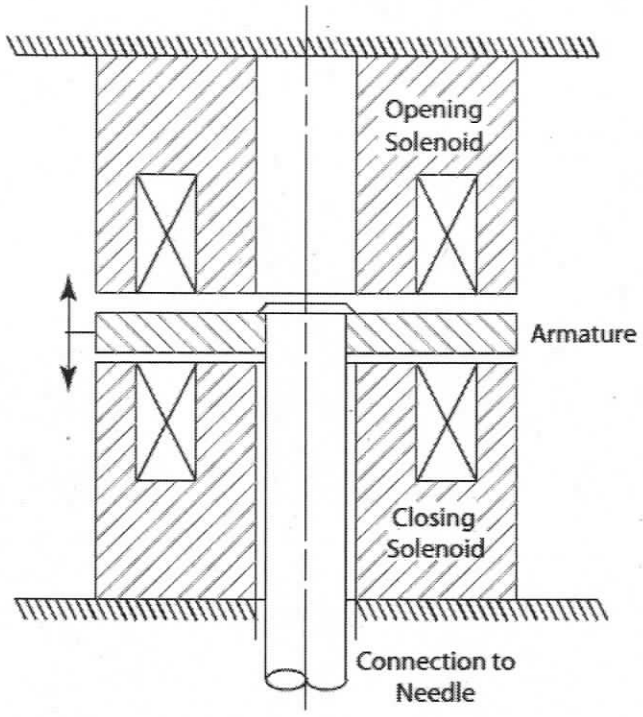

Figure 2-7: Double-acting actuation principle.

This solenoid is energized after the opening solenoid has been de-energized and applies a closing force on the armature. The force applied by the solenoid once the needle impacts the seat is sufficiently large that, on impact, the armature is held in place, nearly eliminating injector bounce, as shown Figure 2-8, which shows the current and lift profiles of a DA injector.

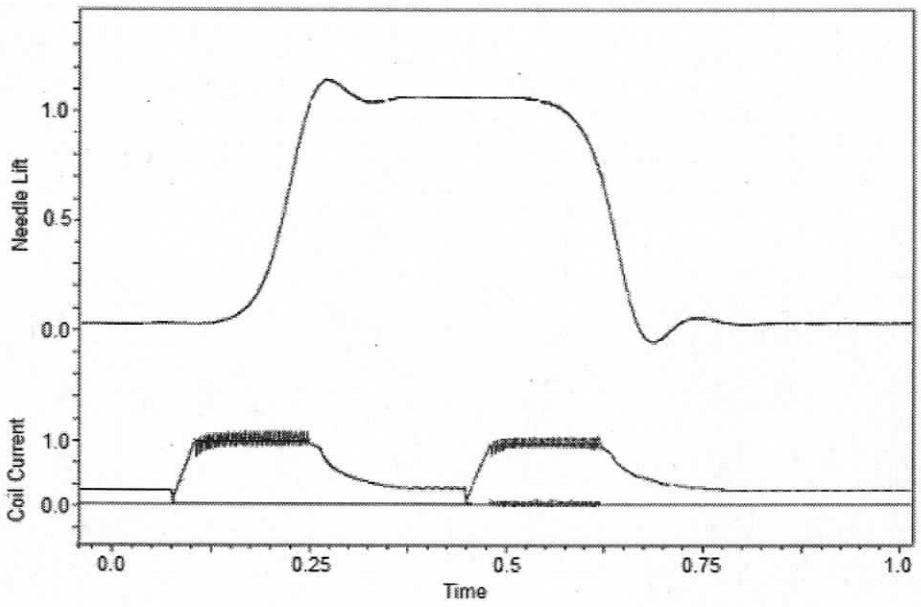

Figure 2-8: DA solenoid current and corresponding needle motion.

The DA concept solves the low pressure direct injection problem previously discussed, by using the lower magnet to hold the injector closed during the compression and combustion cycle of the cylinder. Another advantage of DA technology is that the closing of the injector is faster due to the addition of the second solenoid which allows for better control of the air-fuel ratio in the cylinder. The operation in ballistic mode, where the injector is not allowed to fully open before closing again, can also be achieved by overlapping the closing and opening solenoid current signal. As the needle begins to move, the opening solenoid current is cut off. At the same time, the closing current is building which pulls the injector closed. This procedure has been tested, but results have shown that the cycle-to-cycle variance is large, and so some type of stroke feedback is required to operate reliably in ballistic mode.

2.4.1 Double Acting Solenoid Control

The engine controller produces a PWM signal based on engine speed and load where the pulse width determines the amount of time the injector remains open. The injector booster then produces a corresponding peak hold current signal as shown in Figure 2-9. The booster itself has a lag, known as the response time, at both the start and end of the

signal which is caused by the time it takes the booster to register a change in the PWM signal. This lag is usually around 0.1ms. The opening time is determined as the total time, including closing lag, that the solenoid has current flowing through it. The peak and hold currents parameters are stored in flash memory in the booster as well as the peak time, boost time, and boost voltage. The slope of the current increase to the peak current is dependant on the impedance of the coil. To increase the rate of current increase, most boosters apply a voltage of 45 or 90 volts for a short period of time at the beginning of a pulse and which helps the current overcome the coil impedance. The peak current drops down to the hold current after a specified amount of time because the injector is now open and does not require high forces to remain open. This saves power and reduces the heat generated in the solenoid winding. The hold current drops to zero once the electronic booster detects the end of the PWM pulse. In the case of a DA booster, the detection of the end of the PWM pulse also triggers another peak-hold current signal in the lower solenoid which pulls the injector closed. The DA booster can also apply current to the lower solenoid during combustion to ensure that low pressure injectors remain closed.

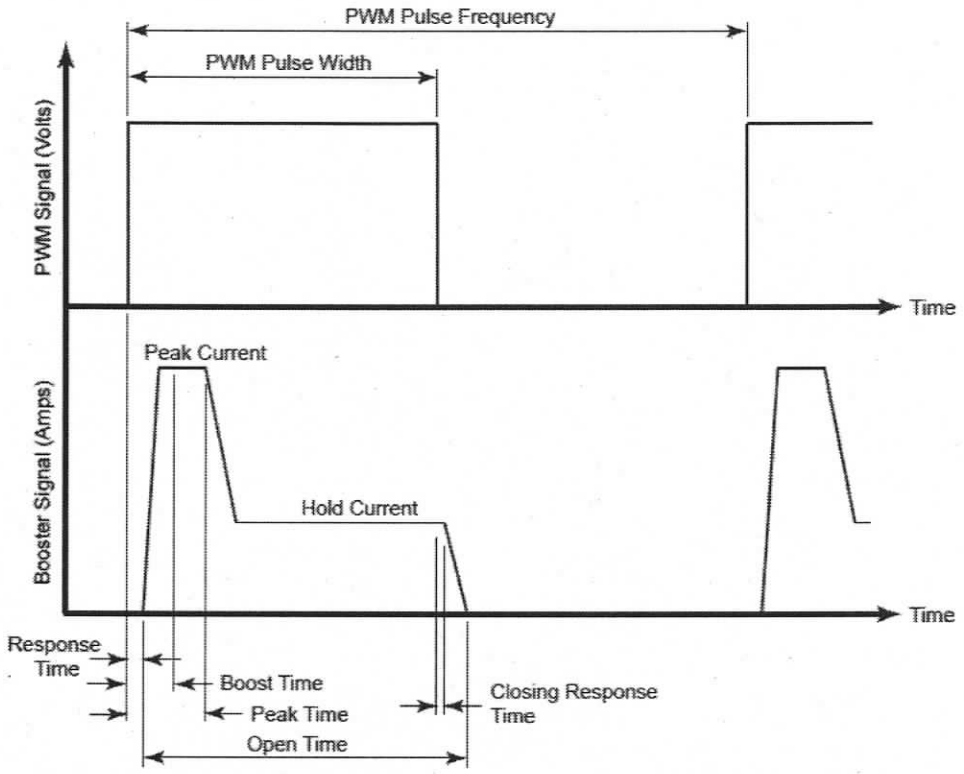

Figure 2-9: Typical electromagnet current signal.

2.4.2 Double-Acting Needle/Seat Geometries

The DA technology can be applied to range of injection applications from high pressure (100-300 bar), middle pressure (20-90 bar) and low pressure (5- 20 bar). Figure 2-10 shows the respective sealing geometries used for each pressure range. The high pressure geometry, as shown in Figure 2-10 (A), is a typical needle/seat combination where DA technology is applied to increase injector closing speed as well as reduce needle bounce. The geometry shown in Figure 2-10 (B) is known as a valve plate and ring seat design. The seat consists of one or more concentric rings which are sealed by a valve plate. This design is used for middle pressure DA injectors in order to compensate the large flow area and high combustion pressure. Finally, the outwards opening low pressure design shown in Figure 2-10 also accommodates large flow areas by adding concentric rings. DA technology is used in these low pressure applications to increase the closing speed of the injector. It is not used for applying a closing force because the outwardly opening

design uses the combustion pressure to apply the sealing force.

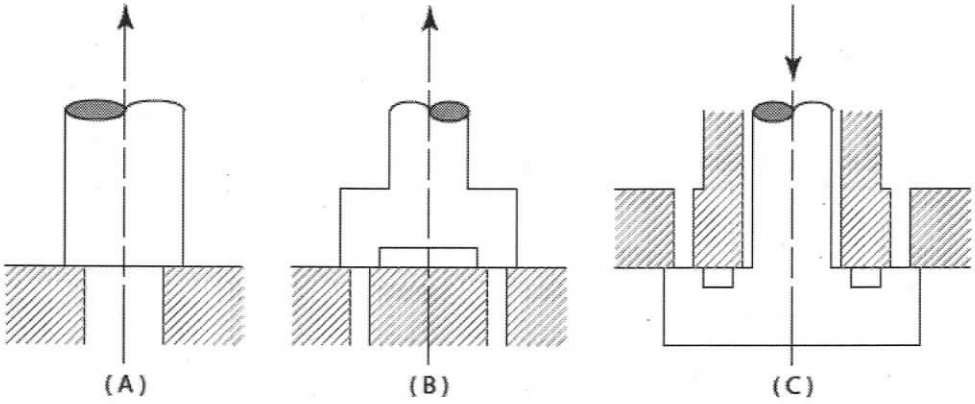

Figure 2-10: Sealing geometries for DA injectors.

The advantage of using flat sealing surfaces as opposed to conical designs is the ease of manufacturing the fine surface conditions required to seal hydrogen, as well improving wear resistance due to the lack of relative motion between components.

Chapter 3 Solenoid Static Force Modelling

The DA injector uses solenoid actuators to open and close the injector against the force acting on the injector needle. The layout of an injector design requires that the engineer know the maximum force which the solenoid can produce at a given distance between the armature and solenoid. The distance is the sum of the injector stroke and solenoid armature rest gap. The injector stroke is calculated based on the injector flow rate requirements, and the rest gap, which ensures no collision between armature and solenoid during injector opening. The following discussion describes development and validation of a static force solenoid model. The current core geometry and material combination is used to validate the model by comparing measured and simulated forces. In addition to the current material combination, other materials with cost or performance advantages will also be compared. This comparison will allow engineers to choose suitable materials based on performance and cost requirements for future solenoid designs. A discussion of the materials and their advantages is given in Appendix A.

3.1 Solenoid Force Measurement

The performance of solenoids for gaseous fuel injection systems can be split into two parameters: static force and dynamic response. Static force is the maximum force between the core and the armature. The static force determines the maximum injector pressure difference which can be opened against given a certain pressure area, injector lift, and current amplitude. The static force is also important when the injector is in the open position as it determines the maximum hold current.

The static force of a solenoid is measured using an apparatus as shown in Figure 3-1. The apparatus consists of three main components: the base, column and plunger. All components were manufactured from steel and designed to minimize deflection. The base sits atop the table of a milling machine and has a precision machined surface where the solenoid can be fixed from behind. Two grooves machined in the bottom of the base allow electrical cabling to pass underneath the apparatus and connect to the solenoid. The column is a steel cylinder which separates the base and plunger. It has two grooves which

provide access of the load sensors' electrical contacts. The concentric alignment of the base in reference to the plunger is essential in order to ensure that the solenoid and armature are concentric as they would be in an injector. The parallelism of the column ends and the base contact surfaces are machined to 0.005 mm to ensure that the solenoid and armature are parallel. Originally, the apparatus was designed without the disk springs, but initial measurements showed that the milling machine bearing slip influenced the measurement results. To solve this problem, two disk springs with a combined force of 3000N were added. The disk spring force added the needed tension to the milling machine bearings and eliminated the slip.

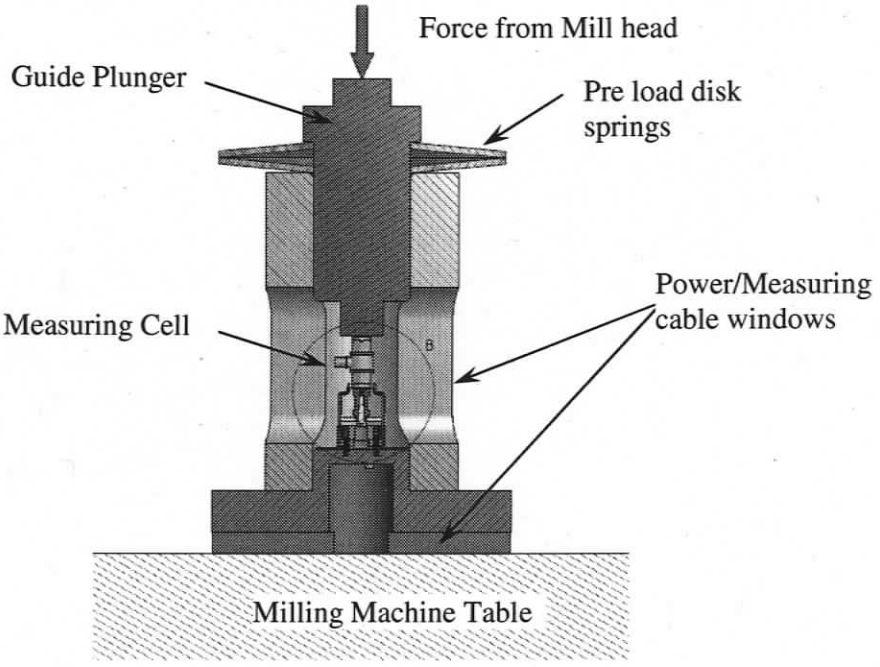

Figure 3-1: Apparatus for solenoid force measurement

The measurement cell as shown in Figure 3-1 consists of the solenoid mounted to the base with electrical connections either in the upward direction or downward through the base. The load cell used to measure the force is a quartz-based force sensor manufactured by Kistler; its specifications are listed in Figure 3-2. This sensor was selected because of its accuracy, as well as the precision of the machined connection surfaces, which is important for proper alignment between solenoid and armature.

Sensor : Kistler Typ 9301B
Type: Quartz Force Links
Specification:

Measurment Range:	± 2.5KN
Sensitivity:	≈ -4 pC/N
Threshold:	≤ 0.02N
Linearity:	≤ ± 0.5 %FSO
Hysteresis:	≥ 0.5 %FSO
Temperature Coefficient	-0.02 %/°C
Operating temperature range:	-40 ... 120 °C

Figure 3-2: Kistler sensor specification [15].

The solenoid is triggered using a valve booster which for this application produces a square current pulse with a boost voltage if 90V, peak current time of 4ms, and no hold current. When the booster is triggered through the application of a single PWM pulse, the force between the solenoid and armature are measured by the load sensor which produces a voltage signal. This signal is measured using a data acquisition system which determines the force.

Before measurement can begin, the system must be zeroed, which can be done using two methods. The first method involved sliding a thickness gauge back and forth between the solenoid and armature while slowly lowering the plunger until the thickness gauge resists motion. This method turned out to be inaccurate, non repeatable and time consuming. A simpler method was developed whereby the plunger was lowered until the force sensor registered a signal; the plunger was then backed off until the sensor returned to zero. This method proved to be repeatable, but caution must be taken not to over-compress the sensor as it can easily be damaged. Once zeroed, the distance between solenoid and armature was tracked using a digital depth gauge connected between the milling machine head and base.

3.1.1 Static Force Measurement Results

Figure 3-3 shows the results of a full measurement sweep using the apparatus described

in the previous section. A complete sweep involves setting the gap between armature and solenoid and varying the current values. The dark lines indicate lifts, which are standard values used for calculation and simulation of injectors. It is important to remember that when using these plots, the minimum air gap is included. This means that if the force produced by the solenoid at certain lift is of interest, the rest gap must be added before reading the force curve.

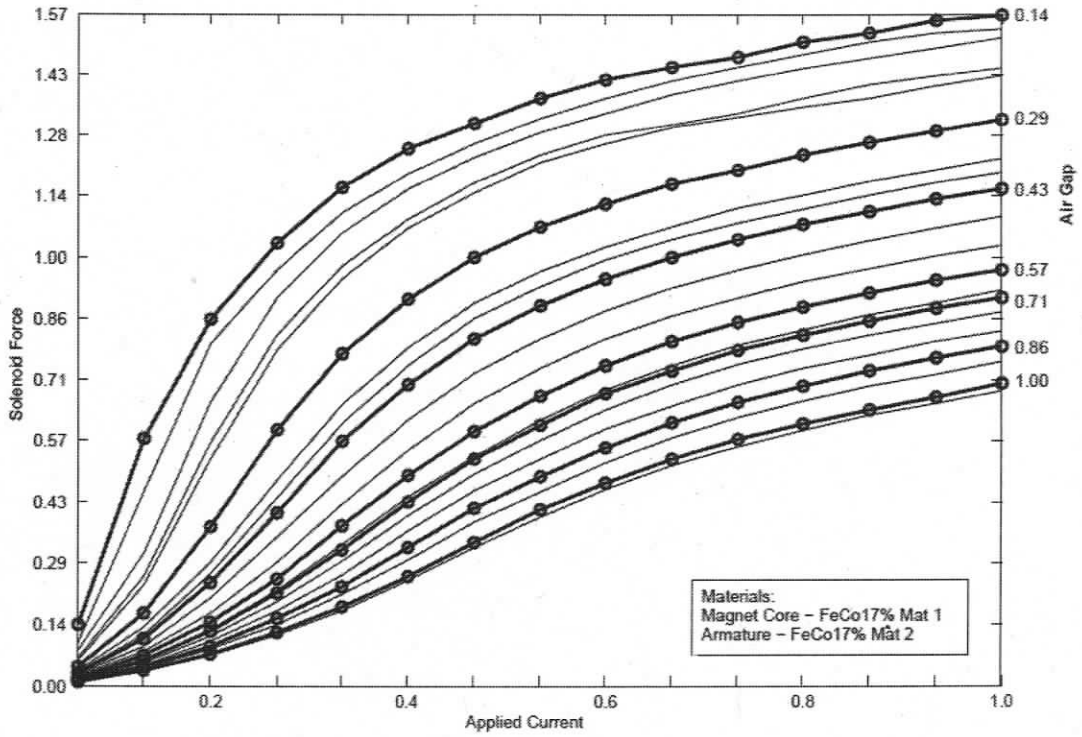

Figure 3-3: Typical current vs force, lift plot.

Figure 3-4 and Figure 3-5 show a comparison between a number of different materials (see Appendix A for a detailed description of each material.) Figure 3-4 shows the forces measured with a large gap between solenoid and armature. From the slope of the curves it appears that the materials are nearing saturation as the slopes are starting to flatten out. From the figure we can see that the two iron-cobalt alloys have similar responses over the entire range. It should be noted that the FeSi3% Mat 1 measurements were carried out using a FeSi3% Mat 2 armature due to the unavailability of FeSi3% Mat 1 which was assumed to have similar magnetic properties. However, subsequent sections will show

that this is not true, and in this case the armature material is limiting solenoid force potential. The plot also shows that the FeSi3% material performs marginally better at lower currents than its cobalt alloy counter parts. At higher current values the FeSi3% enters saturation sooner than the cobalt alloys, which is represented by a levelling of the FeSi3% curve. The figure also shows that both FeSi1% and the tool steel perform well in low current ranges, but, as the current increases, the material quickly becomes saturated, and the force levels off.

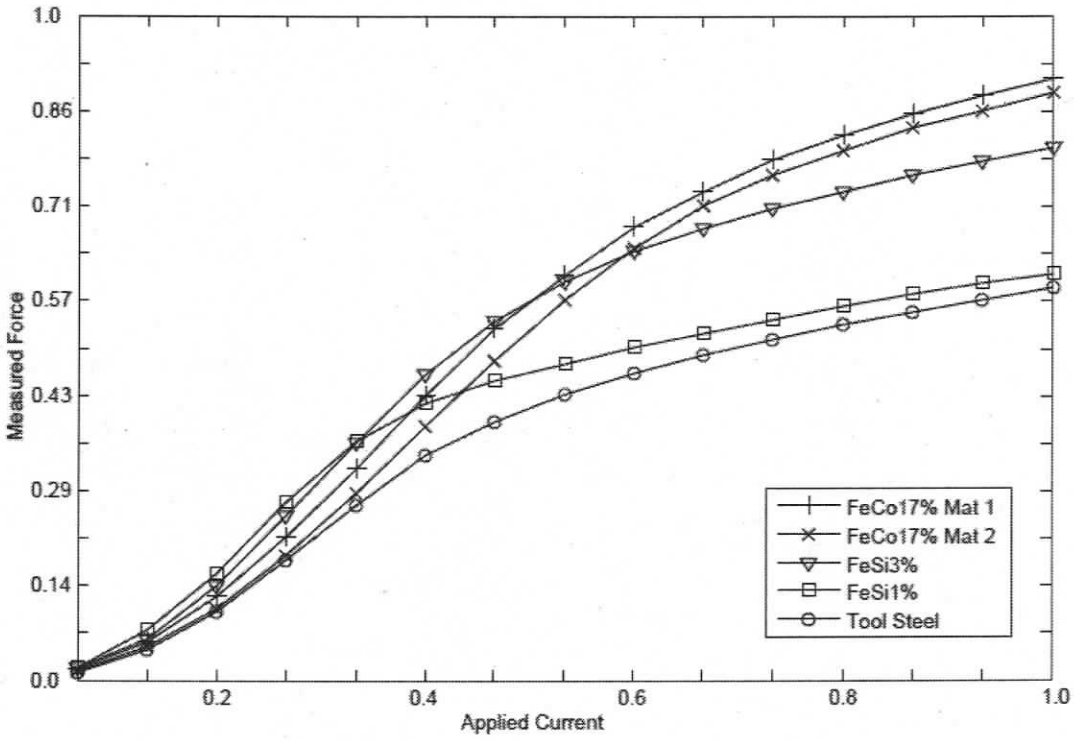

Figure 3-4: Force comparison where solenoid and armature gap is large.

Figure 3-5 shows the plot of the measured magnetic force at a small air gap. Again from the figure, it can be seen that the two cobalt alloys show similar performance except that the FeCo17% Mat 1 shows better low current performance. The FeSi3% material performs better than the cobalt alloys at low current values, but once the current values increase, the material quickly transitions into the saturation region and the force curve levels out. The same is true for FeSi1% and tool steel; both materials quickly enter the saturation region when the current increases above 0.4.

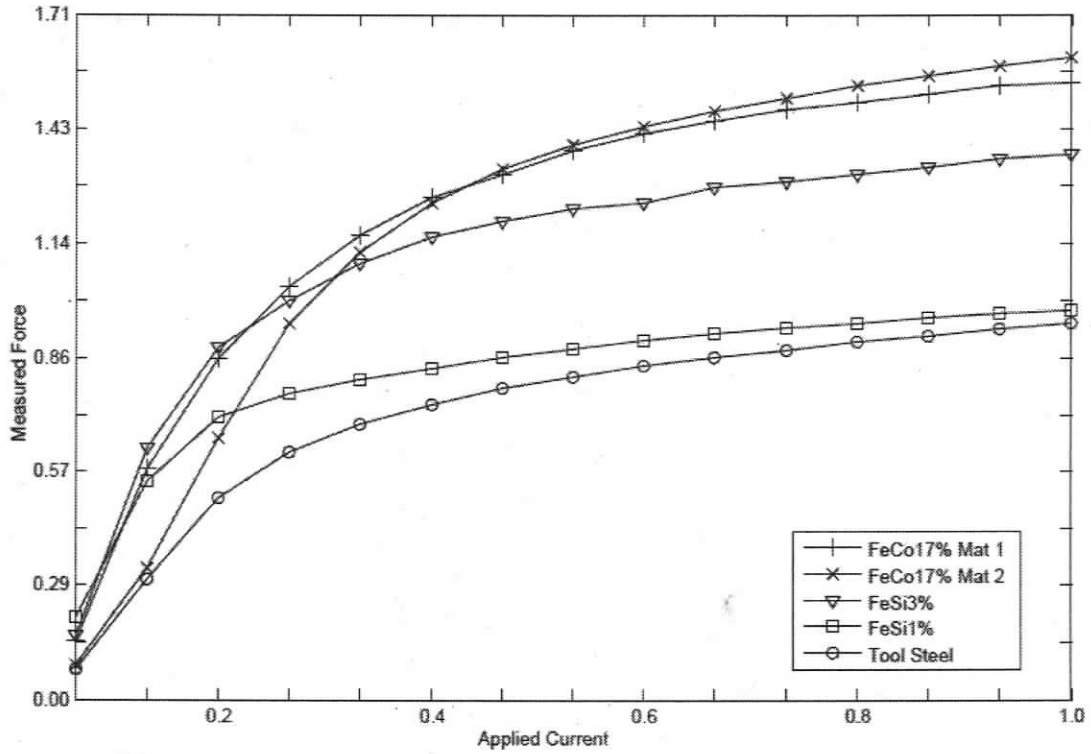

Figure 3-5: Force comparison where solenoid and armature gap is small.

Based on these results, it can be seen that the FeSi3% material would be a good replacement candidate for the expensive cobalt alloys. The cobalt alloys have higher forces than the FeSi3% material in cases of high current/saturation levels. However, most applications limit current to a range below where this would be an advantage. It can be seen from both figures that in the lower current range the FeSi3% material is comparable and in some cases even exceeds the cobalt materials.

3.2 Material B-H Curves

The key material property needed to model a solenoid is the core and armature material permeability. As discussed in Appendix A, permeability is not a constant and is characterised by a B-H curve.

The magnetic permeability of selected materials was determined by Munich's Technical University's Walther-Meißner-Institute. The measurements needed to generate the B-H curves were performed using a SQUID magnetometer. An overview of the apparatus,

operating principles, and sample geometry is given in Appendix B.

Figure 3-6 shows the resulting B-H loops of the selected materials. From the loops it can be seen that, as expected, tool steel has the lowest performance and has a saturation magnetic induction around 1.6 Tesla. The tool steel also depicts high hysteresis losses, as shown in Figure 3-7, which result in remanence within the material. This remanence can have an effect on the closing time of an injector in cases where the return spring force is small. The two cobalt iron materials show maximum magnetic inductions of approximately 2.5 T and 3 T respectively. The difference between these materials which have similar compositions is attributed to differences in the heat treatment processes. The heat treatment process of the FeCo17% Mat 1 was not performed according to manufactures specifications and will be discussed in following thesis sections.

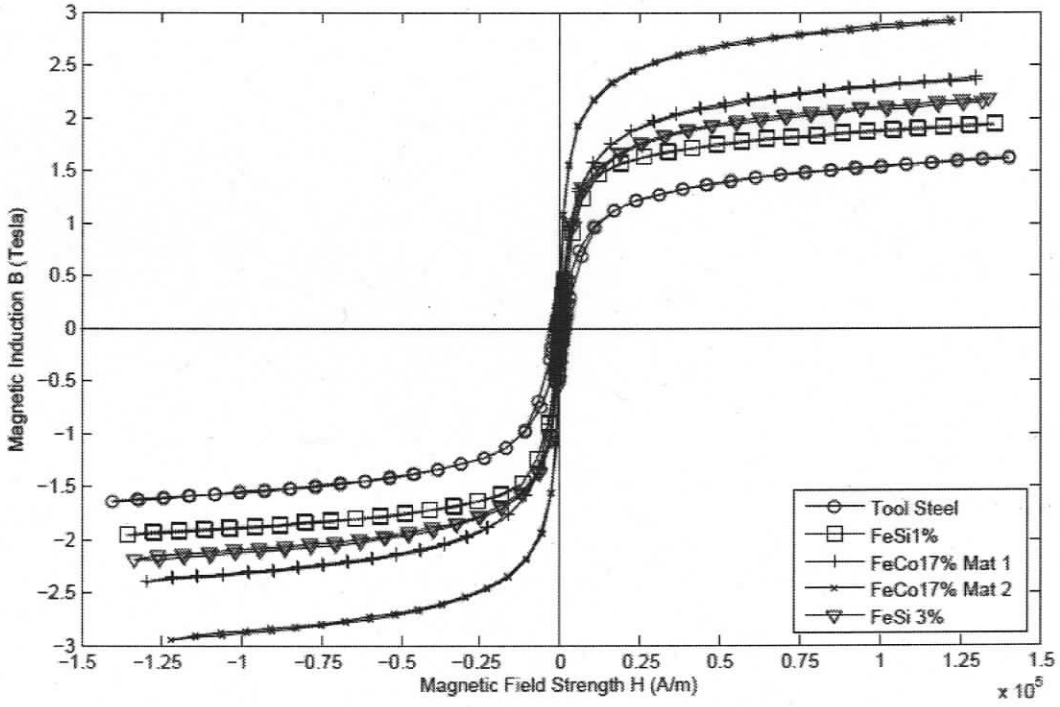

Figure 3-6: B-H loops for selected materials.

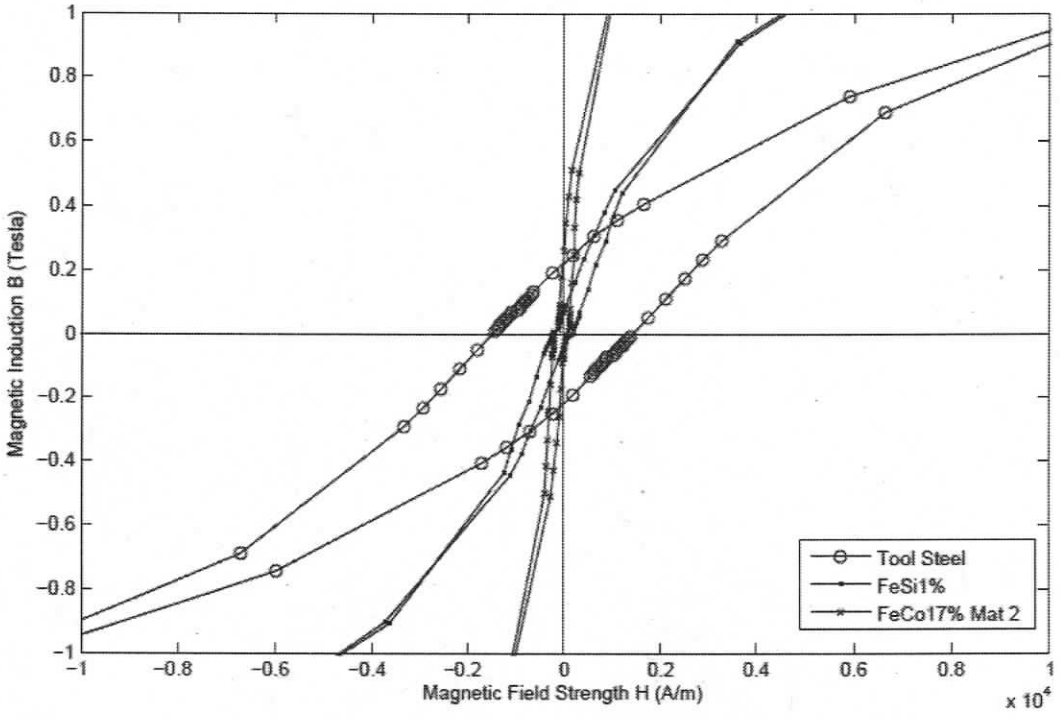

Figure 3-7: B-H loop hysteresis of selected materials.

The conversion of B-H data to permeability as a function of B is performed using Equation 3.1

$$\mu_r = \frac{B}{\mu_o H} \tag{3.1}$$

If the entire B-H Loop is calculated, a plot of permeability can be generated which spans all 4 plot quadrants. For the simulations, we are only interested in the permeability of the material in the first quadrant between the positive x and y axes of B-H diagram. Within this quadrant there are two curves. The first curve is the initial magnetization curve which started at 2000 Oe and went to -2000 Oe, whilst the second curve is the returning curve back to positive 2000 Oe. For the simulations the returning curve was used to define the material permeability.

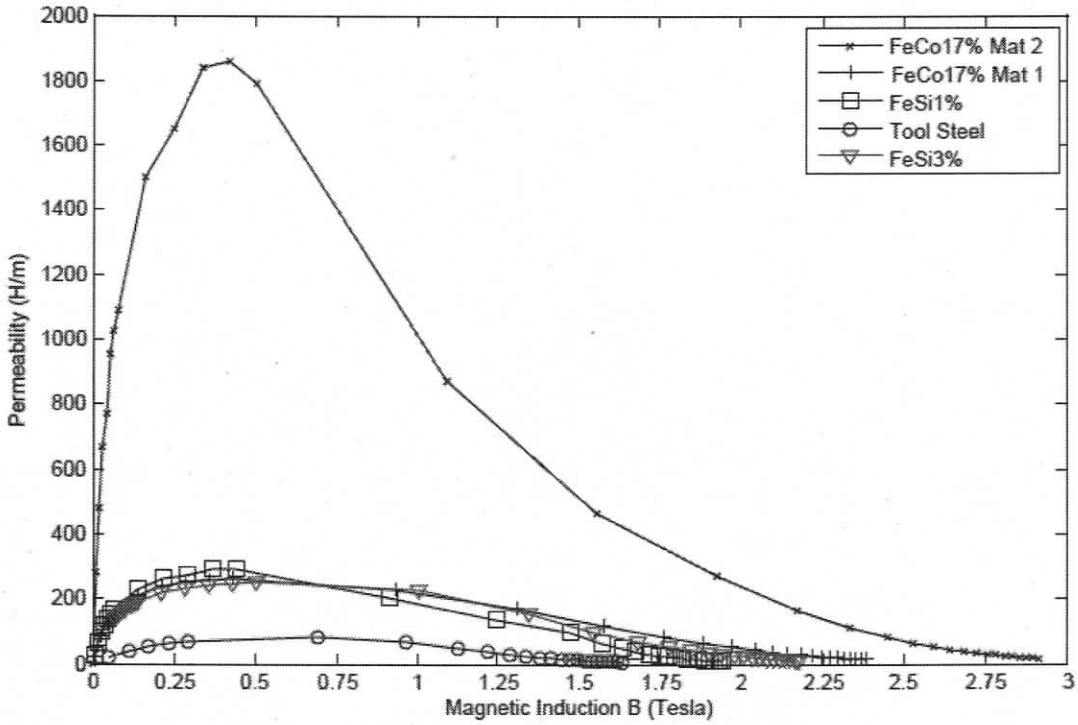

Figure 3-8: Permeability of selected materials.

Figure 3-8 shows the permeability of the selected materials. It can be seen that FeCo17% Mat 2 has the highest permeability, while a similar material (in terms of composition) FeCo17% Mat 1 has a much lower permeability. Further investigations with the material supplier determined that the heat treatment process used was incorrect and did not follow the manufacturer's guidelines. The heat treat was performed according to the following procedure:

Oven Temperature - 850°C ± 10°C for 10 hours

Atmosphere – Vacuum

Cooling Rate - 100°C/hour to 200°C then air cool

The manufacturer specifies the same procedure except that the instead of a vacuum, a dry H_2 atmosphere is specified. The heat treatment of the FeCo17% Mat 1 material was modified to save costs under the assumption that the heat treatment process was primarily used to develop a specific grain structure in the material which is not atmosphere dependant. However, further investigation revealed that the hydrogen atmosphere was specified not because of material structure, but rather as a decarburizing atmosphere. Iron

cobalt has poor mechanical properties, which makes it hard to machine. To solve this problem the manufacturer adds carbon to the steel which decreases ductility but increases tensile strength. However, carbon significantly reduces the magnetic properties of the material and hence is not an ideal component of any magnetic material. To solve this problem, the manufacturer specifies the H2 atmosphere since hydrogen reacts with carbon on the surface of the material to form methane according to the following chemical reaction:

$$C(Fe) + 2H_2 \Leftrightarrow CH_4$$

The removal of carbon from the material surface allows internal carbon atoms to move to the surface in order to maintain equilibrium. This reduces the tensile strength, hardness, and creep resistance but increases ductility. However, this process can have unwanted side effects if the material is not homogenous in which case hydrogen will diffuse along grain boundaries and react with the internal carbon to form methane which gathers in voids in the metal matrix. The accumulation of gases in the internal voids can cause high local stress, leading to cracks in the material. With extended exposure to high temperature hydrogen, the material will eventually become starved of carbon, and any methane trapped within the voids will react back into the material and travel to the surface.

Figure 3-9 shows a comparison between the measured FeCo17% Mat 1 permeability and the permeability curve provided by the supplier. It is important to mention that the manufacturer data describes the initial magnetization curve, which explains the shift to right. The figure shows that although the high material price is being paid, the maximum material potential is not being utilized. The measured data will be used to verify finite element model results.

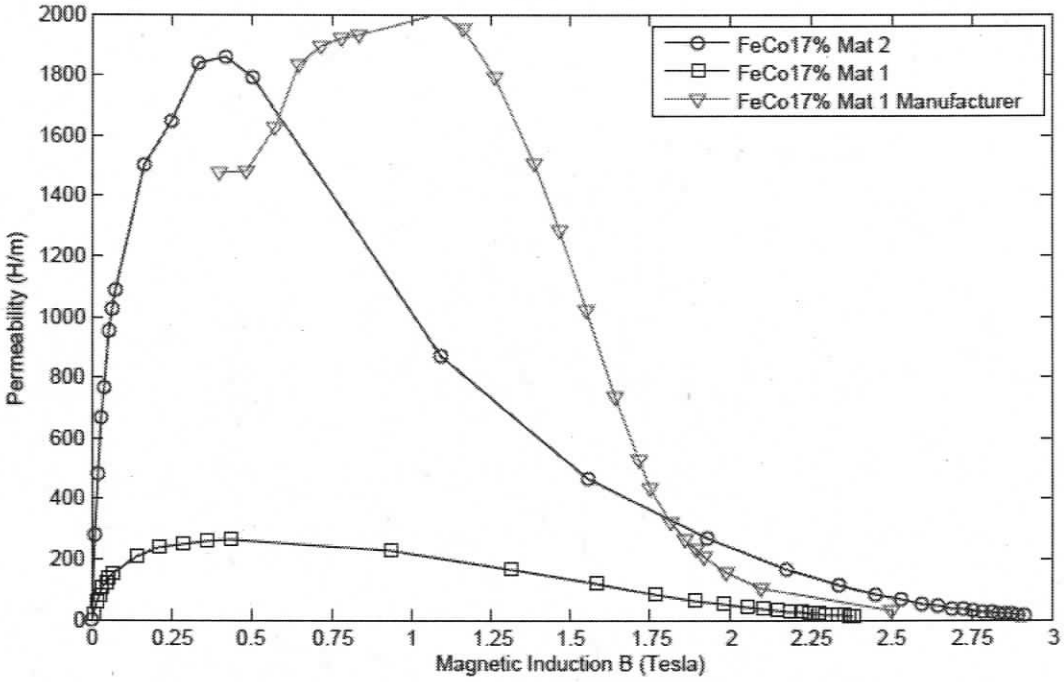

Figure 3-9: FeCo17% Mat 1 manufacturer's permeability data.

For the application of solenoids, the permeability at high magnetic inductions is of most interest. It can be seen that the results of the permeability of the different materials correlate with the measured force maximums presented in previous sections. For example, it was shown in Figure 3-5 that at low currents the resultant force generated by FeSi1% was higher than that of FeSi3% and FeCo17% Mat 1. This result is consistent with the data in Figure 3-10 (showing data for lower inductions only) since at low magnetic induction, FeSi1% shows the highest permeability.

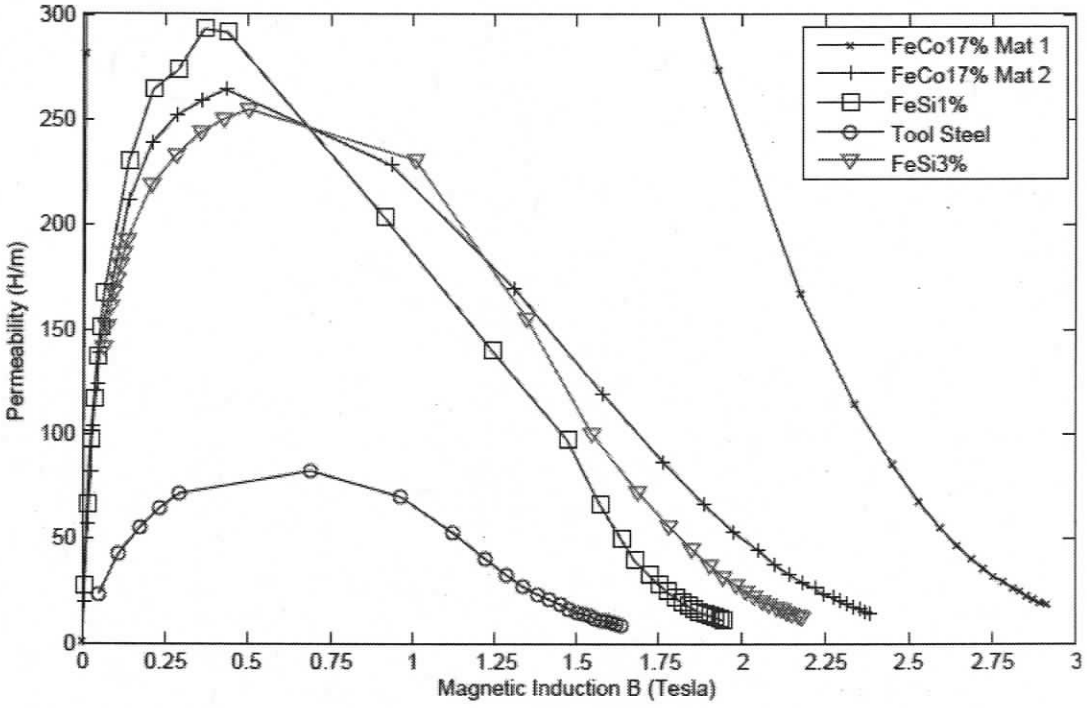

Figure 3-10: Permeability of selected materials.

3.3 Electromagnet Finite Element Model

3.3.1 Magnetic Core Layout

The layout of a magnetic core is an iterative process with the goal of optimizing the usage of material properties while conforming to dimensional and/or force requirement constraints. There are two factors which define the force output: the coil and the solenoid core face surface. Coil parameters, such wire diameter, number of windings and radial position, define coil resistance and material saturation. The coil must be dimensioned to provide a low electrical impedance to increase solenoid dynamics and reduce coil temperature. The face surface of the solenoid on either side of the coil should be calculated so that the inner surface is equal to the outer surface which ensures that the magnetic flux remains within the core. The challenge is then to position and size the coil in such a way that the face surfaces are saturated at a given current, while also ensuring that the coil electrical resistance remains at a reasonable level.

3.3.2 Finite Element Model

The modelling of the solenoid used in the DA injectors is shown in Figure 3-11. This model is a simplification of the core and armature used in DA injectors. It is assumed that the solenoid is rotationally symmetric, neglecting any connection or injection-moulded geometry. The coil does not fill the window of the magnet core because it is held in place by the coil holder which is fixed by the injection-moulded fill material which is non-magnetic and so neglected by the model.

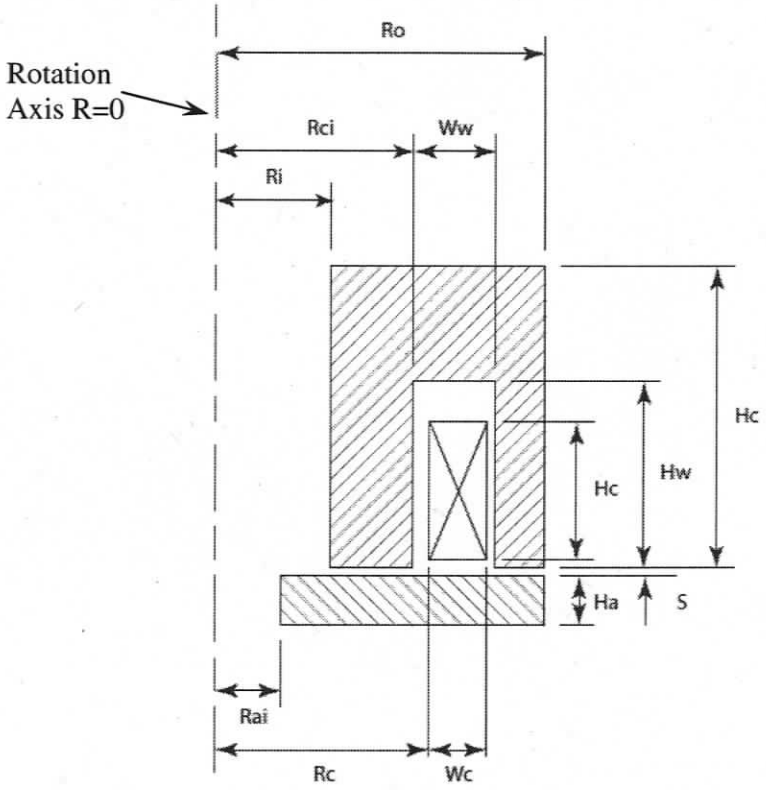

Figure 3-11: Finite element model.

Table 3-1: Finite element model parameters

Variable	Description
Ro	Outer solenoid radius
Rci	Inner window radius
Ww	Window width
Ri	Inner solenoid radius
Rai	Inner armature radius

Rc	Inner coil radius
Wc	Coil width
Hc	Core height
Hw	Window height
Hc	Coil height
Ha	Armature height
S	Core armature distance

The simulations were performed in Comsol using the Azimuthal induction currents mode from the AC/DC module. This mode is used for magnetostatics of conducting and magnetic materials with electric currents flowing in the angular direction in and out of the page [16].

Once the model geometry is defined, the coil current density is determined. The current density can be calculated by knowing the winding cross-section, the number of turns making up the coil, N, and the current, i, as defined by Equation 3.2.

$$\varphi_{coil} = \frac{N \cdot i}{h_C w_C} \tag{3.2}$$

The coil's magnetic permeability is assumed to be 1. The core and armature material permeability are defined as functions of flux density and are determined according to the method described in Appendix B. The model area is also bounded by a box, and its parameters are set to that of air. The boundary conditions are set as magnetic insulation.

3.4 Results of Finite Element Model

The results of the finite element model are presented in Figure 3-12 and Figure 3-13 which depict the comparison between measured and simulated force at large and small gap between solenoid and armature. The results show that the simulation for FeCo17% Mat 1, FeSi1%, and FeSi3% have comparable magnitudes as compared to the measured data to within ±5% over the current range. However, the other two materials FeCo17% Mat 2 and tool steel show a large difference between measured and simulated. The difference in the FeCo17% Mat 2 force values can be explained by the fact that the

armature used to measured the force was made of non-heat treated FeCo17% Mat 1, which was the limiting material in the force measurement. This is why the measured data for FeCo17% Mat 1 is similar to that of FeCo17% Mat 2. The difference between the measured and simulated tool steel forces is attributed to a variation in the material structure. Although both materials underwent heat treatment, the difference in sample size used for permeability determination and force measurement resulted in different material structures. Tool steel contains a high percentage of carbon, which makes the material structure heavily dependant on heat treatment.

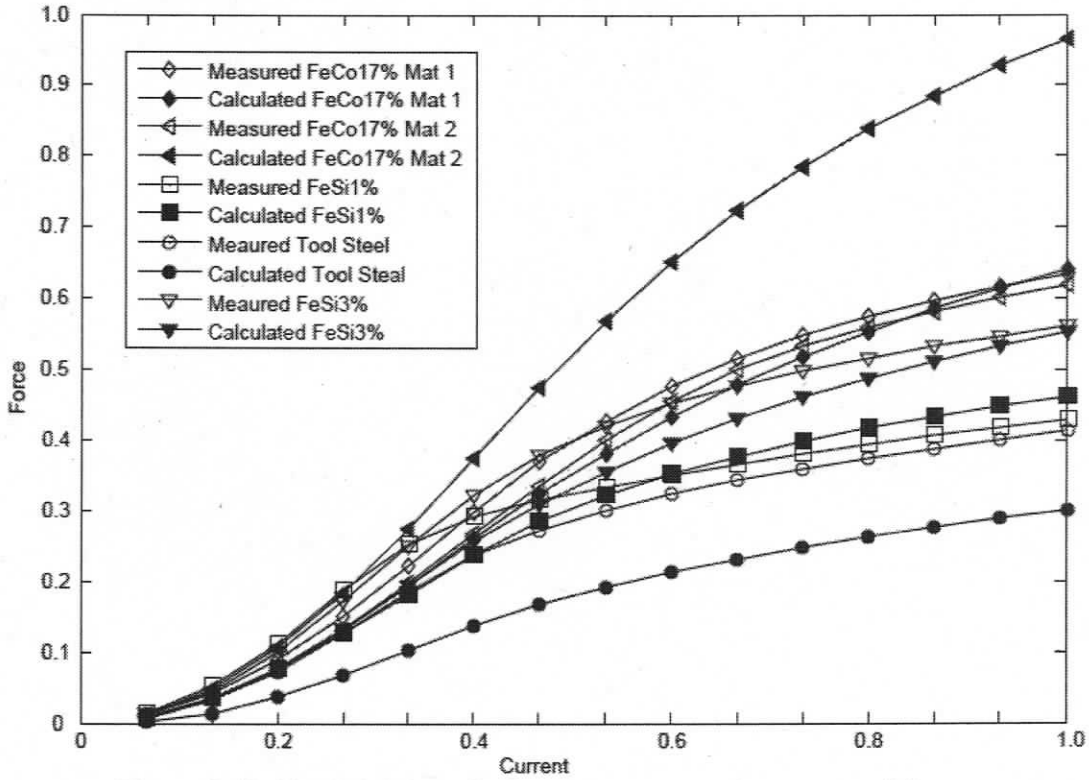

Figure 3-12: Simulated force for large gap compared to measured force.

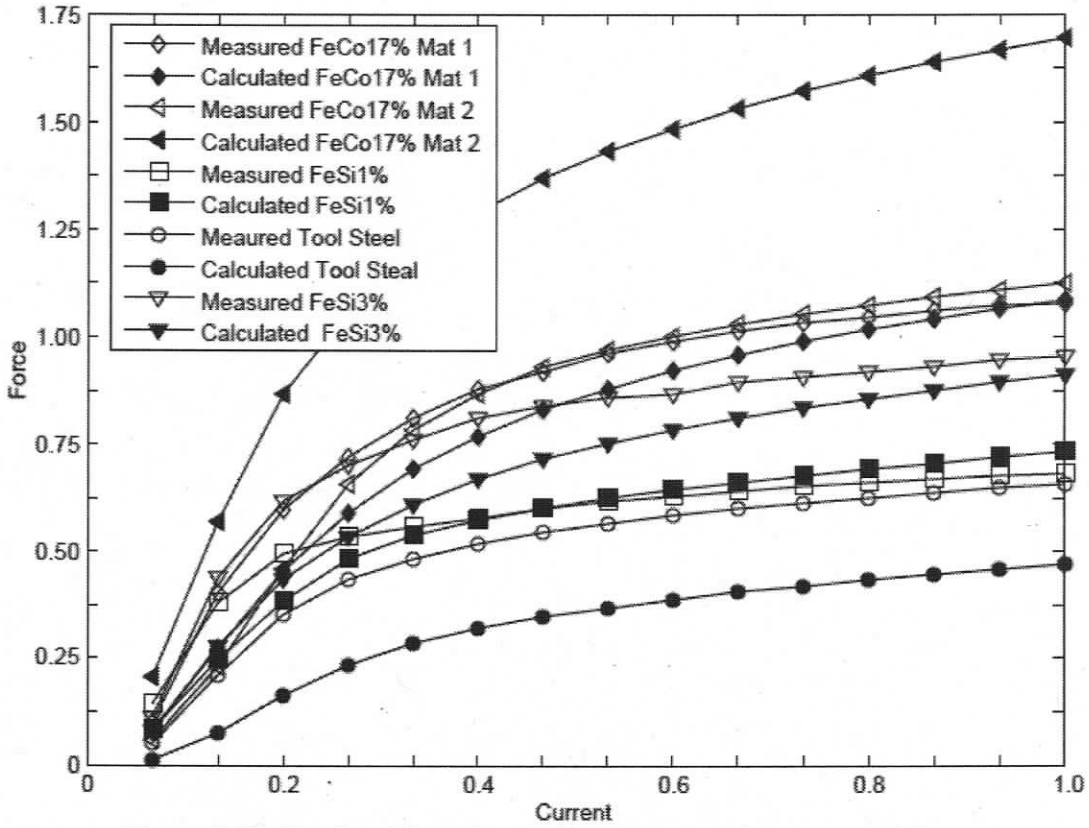

Figure 3-13: Simulated force for small gap compared to measured force.

3.4.1 Sources of Error

The correlation between measured and computed solenoid force is good; however, there are deviations which indicate error in the measurement system, permeability data and/or model geometry. As discussed in previous sections, the measurement of the force using the test apparatus must be zeroed before each measurement. The zeroing process is not exact and relies on experience of the operator. The permeability data for each material is likely the largest source of error due to the dependence of the conversion process on the sample volume. As shown in Figure B-0-3, the sample must be manufactured within specified tolerances and, due the small size of the sample, these tolerances are difficult to maintain. A tolerance analysis of the sample volume shows that through the dimensional tolerances, the volume may vary up to ±6%; if one also accounts for truncation and/or bending of the sample during the manufacturing process, a volume tolerance of ±10% is possible.

Figure 3-14 shows the bounding force curves for FeCo17% Mat 1 where a tolerance of ±10% was applied to the permeability of the material. Variations in the slope of the force curves between measured and simulated can also be explained by slight differences in the heat treatment condition of the material. For example, materials such FeSi1% are not heat-treated after the manufacturing process, which could lead to differences in the material structure of the sample as its small mass was exposed to higher friction generated heat.

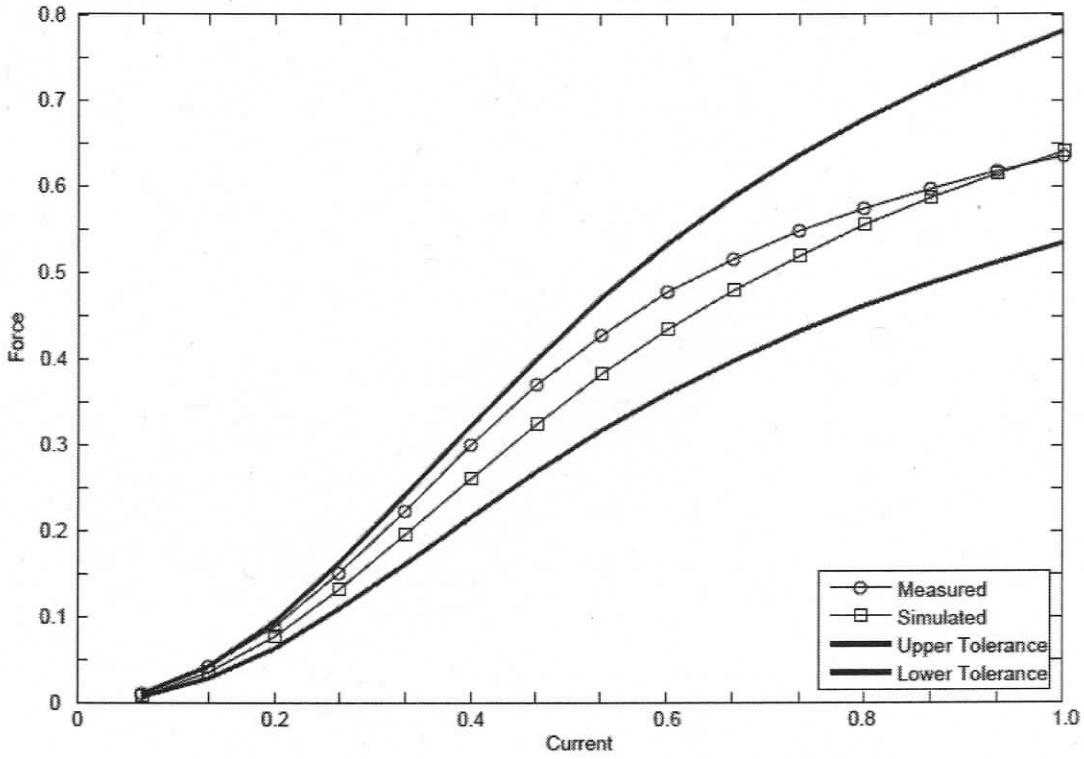

Figure 3-14: Simulated Tolerance Band for FeCo17% Mat 1

Another source of error comes from the model directly because of the assumption that the core is rotationally symmetric. In fact, the core is symmetric except for the slice cut into the face as shown in **Error! Reference source not found.**. The slice changes the ratio of surface areas between the surfaces to the left and right of the coil. This difference in surface areas leads to a decreased flux density at the armature resulting in a lower magnetic force.

The solenoid force model developed above shows that there is a difference between the materials selected for investigation. Using the model results injector designers can optimize solenoid designs for given applications. In the following sections a dynamic lift model will be created which allows DA injector designers to optimize the material and geometric parameters of a new injector design, eliminating the need for prototype revisions The results of the solenoid model developed above will be used to simulated the effect of various solenoid materials on the performance of a DA high pressure injector.

3.5 Summary

The objective of the previous chapter was to develop and validate a model which can be used to predict the force characteristic of the solenoids used in DA injector designs. The model was validated using the solenoid geometry of an existing solenoid by comparing compute results with measured results. The measured results where obtained using a specially designed measurement apparatus. With the help of an external lab material properties required for magnetic simulation where gather for various alternative material which where selected based on performance, cost, corrosion resistance, and machinability. The range of alternative materials allows for the optimization of DA actuation solenoids to meet application requirements such as performance and cost. The solenoid simulations also provide the basis for the DA injection motion model derived in the Chapter 4.

Chapter 4 Dynamic Response Modelling of HDAI

4.1 Modelling Objectives

In this chapter a model predicting the response of DA injectors will be developed. The model allows variation of needle, seat, and stop material as well as pressure, return spring force and solenoid force. Important parameters, such as opening speed, closing speed and impact conditions, will be determined as a function of the various design parameters. The model will also determine the forces at impact with the seat or stop. Using the impact force data, the seat and stop can be optimized in regards to durability before any lifetime testing is conducted. Once the model has been validated by comparison with a measured lift profile, the model will be used to simulate the effect of selected solenoid materials.

4.2 Model Development for DA Injectors

The development of a spring mass damper model begins with analysing the injector geometry to determine where mass is concentrated, which components act as connecting spring damper systems between the masses and which forces act on these masses. Figure 4-1 (A) shows a simple free-body diagram of the injector needle and armature assembly for a DA high pressure injector. Figure 4-1 (B) shows the equivalent spring mass damper model where the mass of the valve plate M_2 and mass of the armature M_1 are connected by a spring and damper. The spring, k_r, and damper, d_r, represent the rod connecting these two components in the actual injector design. The mass of the connecting rod is evenly split between the two masses. Mass M_1 contains the mass of the armature and upper guide as well as the mass of the nut which connects it to the injector needle. Mass M_2 contains the valve plate, closing spring, lower guide ring and the guide ring suspension O-ring. In the event that this model is adapted to other double acting injectors such as low pressure versions, the position of the stop and closing spring may be reversed to fit the injector design parameters.

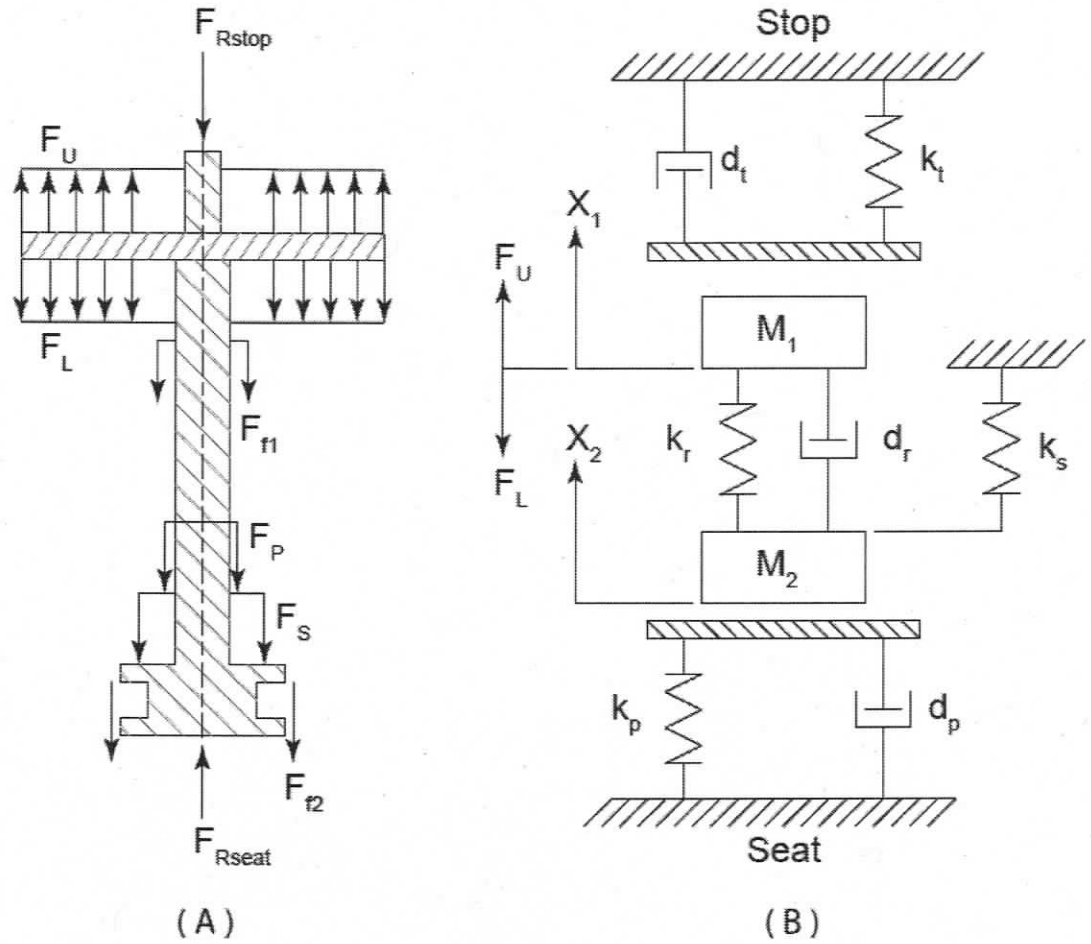

Figure 4-1: Mass spring damper model of a high pressure DAI.

From Figure 4-1 (B) a set of second order differential Equations 4.1 and 4.2 are derived. These equations describe the motion of the injector needle dependant on the internal injector pressure F_P, spring pre load F_{pre}, upper and lower guide friction forces F_{f1} and F_{f2} and upper and lower magnet forces F_L and F_U. The second terms on the left side of equations 4.1 and 4.2 represent the material damping force of the connecting rod between armature and injector valve plate masses. This damping term is considered to be always dissipative in the direction of the mass motion, as indicated by the sign of the velocity component.

$$m_2\ddot{x}_2 + d_r\left|\dot{x}_2 - \dot{x}_1\right| sign(\dot{x}_2) + k_r(x_2 - x_1) + k_s x_2 + F_L + F_{pre} = F_P + m_2 g + F_{Rseat} + F_{f2} \quad \textbf{(4.1)}$$

$$m_1\ddot{x}_1 + d_r\left|\dot{x}_1 - \dot{x}_2\right| sign(\dot{x}_1) + k_r(x_1 - x_2) = F_U + m_1 g + F_{Rstop} + F_{f1} \quad \textbf{(4.2)}$$

The two reaction forces F_{Rseat} and F_{Rstop} are dependant on the following conditions:

$$F_{Rseat}, F_{Rstop} = 0 \qquad \text{for } 0 < x_1, x_2 < H_{MAX} \quad \textbf{(4.3)}$$

$$F_{Rseat} = -k_p x_2 - d_p \dot{x}_2 \qquad \text{for } x_2 \leq 0 \quad \textbf{(4.4)}$$

$$F_{Rstop} = -k_t(x_1 - H_{MAX}) - d_t \dot{x}_n \qquad \text{for } x_1 \geq H_{MAX} \quad \textbf{(4.5)}$$

According to the state of the reaction forces as given in equation 4.3, when $x_2 \leq 0$ is valid, the injector needle has impacted on the injector seat which then acts as a spring pushing back on the injector needle. In the case of $x_1 \geq H_{MAX}$, the injector needle has impacted on the upper stop, which also acts as a spring which applies a force in the opposite direction from the motion. In the case of both the stop and seat, the material damping constants are considered to be always dissipative. To simplify the model, it has been assumed that the steel components, like the connecting rod between the two masses and the seat, provide no impact damping, and so the material damping coefficients are set to zero. The only damping parameter taken into account is in the damping constant of the stop as it is a plastics material which exhibits high impact dissipation characteristics. However, due to the lack of specific information regarding the materials damping constant, this parameter is determined by comparing the results of the simulation to experimentally determined results. The parameters used in the solution of equations 4.1 to 4.5 for a high pressure DA injector are shown in Table 4-1.

Table 4-1: Mass spring damper model parameters

Variable	Description	Value
m_1	Armature mass	0.010804 kg
m_2	Needle mass	0.0031 kg
d_r	Connecting rod damping coefficient	0.0 N-s/m
k_r	Connecting rod spring constant	9.55×10^8 N/m
k_s	Return spring constant	3000 N/m
g	Gravity	9.81 m/s^2
k_p	Seat spring constant	6.45×10^9
d_p	Seat damping coefficient	0.0 N-s/m

k_t	Stop spring constant	1.799×10^7 N/m
d_t	Stop damping coefficient	200 N-s/m

The following sections describe the models used to determine the booster current, solenoid force, injector friction and pressure forces. One aspect that is not discussed further is the drag of the fuel gas flowing past/through the injector components. The drag does add a force which either opposes or aids motion depending on the direction of the needle motion, but, due to the complex geometry and significantly larger solenoid forces, the effect has been assumed to be small and therefore it is not included in the model.

4.2.1 Injector Current Input Model

The booster model used for simulations is shown in Figure 4-2. The model has 5 inputs: time, peak-time, on-time, peak and hold currents, and offset. Peak-time and on-time are given in seconds and currents in amps. The offset parameter simulates the PWM signal by defining when the booster should begin to produce a signal. The only output is the current which is connected to the solenoid model discussed in the next section.

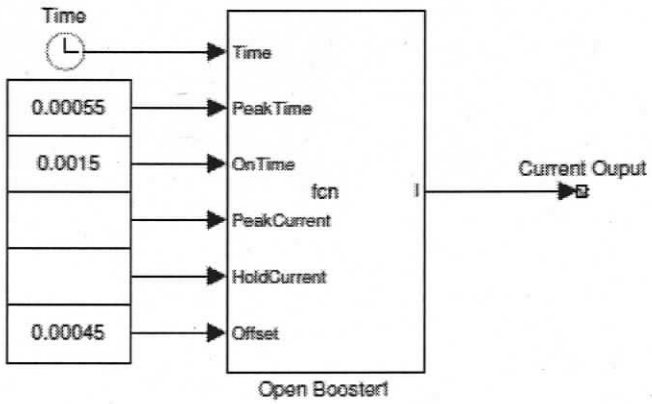

Figure 4-2: Solenoid booster model.

The booster model assumes that the current signal does not need to be regulated once at the peak or hold current and so does not exhibit the two point current regulation that is typical of an injector booster. The second assumption is that the transition from the peak to the hold current is linear. Figure 4-3 compares the simulated signal to a real signal. It

can be seen that the drop in current is an exponential function which is dependant on parameters like coil resistance and inductance. The shape of this transition has no effect on the lift simulation, since at this point the injector is fully open and no longer moving.

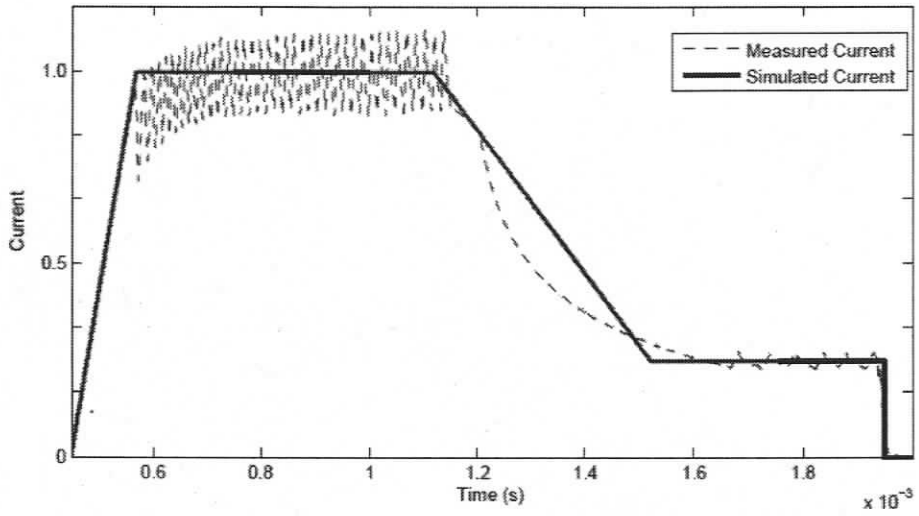

Figure 4-3: Comparison between simulated and measured current.

4.2.2 Solenoid Force Model

The solenoid forces F_L and F_U are the forces applied to the magnetic armature from either the lower or upper solenoid. The upper solenoid applies the force to open the injector, while the lower solenoid applies the force to close the injector. The logic used to determine the magnetic force is shown in Figure 4-4. Using the model results of Chapter 3, the solenoid force can be characterized over a range of armature distances and currents to produce a plot similar to that shown in Figure 3-3. This resulting data is incorporated into a standard two dimensional linear interpolation block as shown in Figure 4-4. The block receives a current input from the current booster and the current distance between the solenoid and the armature as computed by equations 4.1 and 4.2. The input data is then used to interpolate the magnetic force based on the characterization curves of the solenoid.

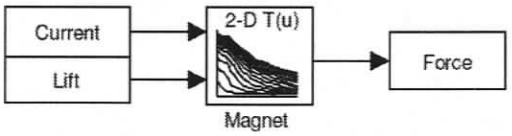

Figure 4-4: Solenoid model block diagram.

Figure 4-5 shows the validation results of the electromagnet model shown in Figure 4-4. Using the current input model, and by setting a constant lift, a force profile was simulated. This predicted force profile is compared to a force profile recorded by the experimental system. The differences between the model and experimental results may be explained by the deviation of the simulated and measured magnetic force as discussed in Chapter 3. It can be seen that the model has a linear response to a change in current, while the measured data shows a non linear start or end before transitioning into a linear increase or decrease of force. This may be explained by the dynamics of a changing magnetic field which is influenced by factors like eddy current which the model does not take into account.

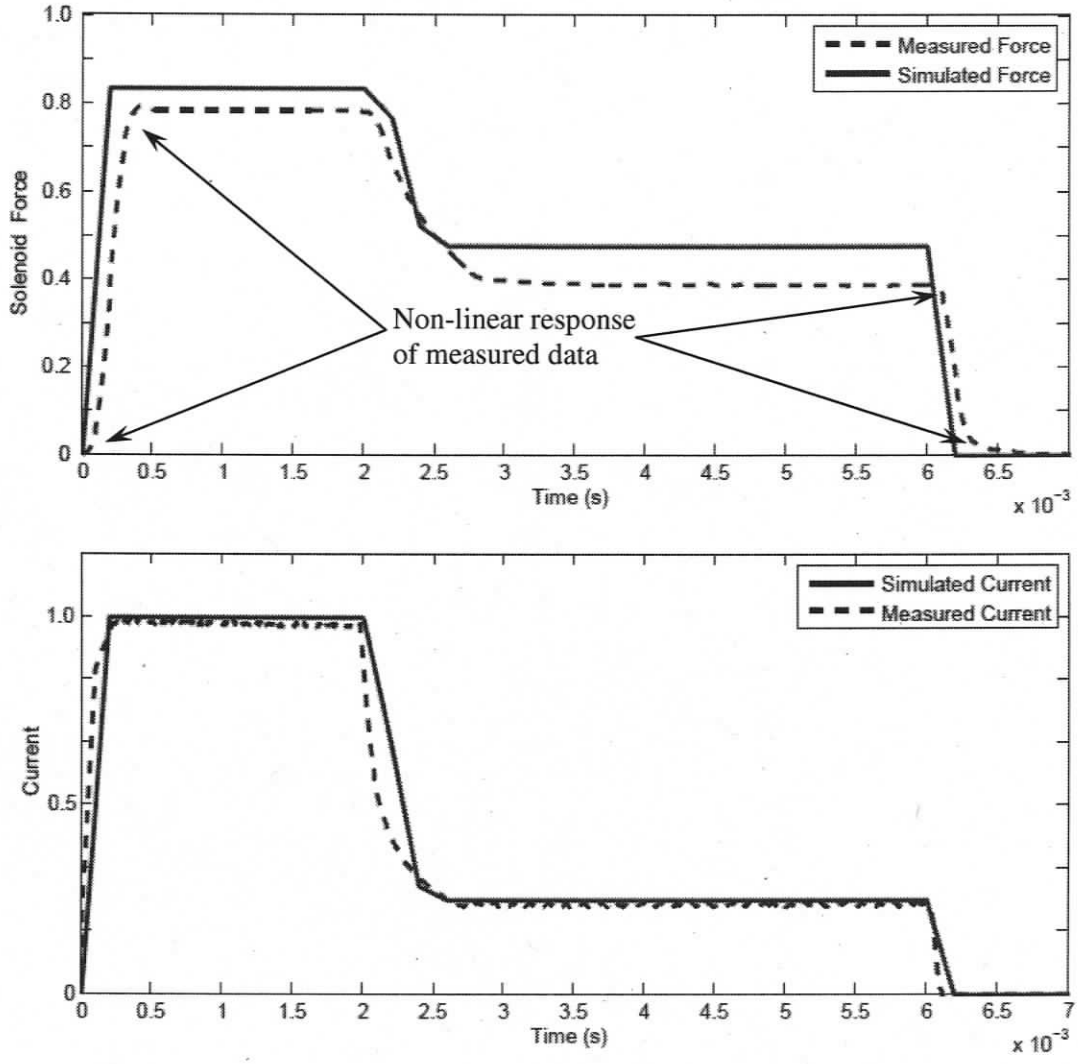

Figure 4-5: Solenoid model results (a) force (b) current.

4.2.3 Injector Friction Model

The friction forces F_{f1} and F_{f2} refer to the friction between the Teflon guide ring and the valves guiding surfaces. All DA injector designs have two guides known as the upper and lower guides. The upper guide is a standard guide ring as shown Figure 4-6 (A). This type of guide is typically only used as a positional guide and so the tolerances are chosen to ensure minimal contact with the guiding surface. The guide itself has a rounded surface which insures that it will have one line of contact and is able tilt to accommodate alignment errors in regards to the sealing surface. The resultant friction force of this type of guide is assumed to be negligible and is not included in the injector lift model.

The second type of guide shown in Figure 4-6 (B) is considered an elastic guide, and it is comprised of two components: the guide ring and tension ring. The guide ring is typically a closed ring which is pressed against the guiding surface by the tension ring typically taking the form of an O-ring. The O-ring applies a constant normal force to the guide ring, which ensures constant contact pressure round the circumference of the guide. This type of guide has the advantage that it acts as an automatic center as well as allowing the guided component to tilt in order to accommodate for errors in the alignment of the injector. It is assumed that this guide is the only significant source of friction within an injector.

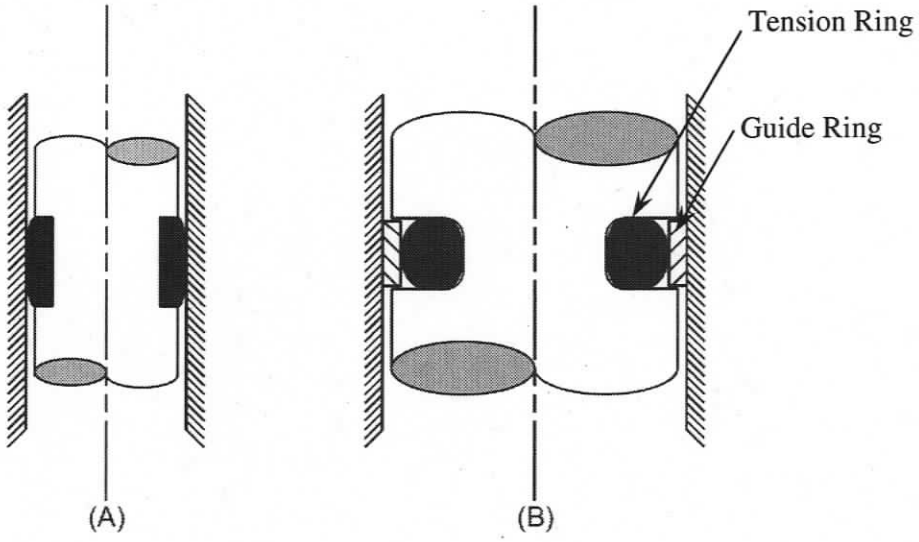

Figure 4-6: Injector guiding methods

A transitional friction model between two surfaces can be applied to describe the resultant friction force between the flexible guide and the guiding surface. The frictional model used is taken from Armstrong [18] and is available in Matlab through the Simscape application. This is incorporated in the injector lift model.

The transitional friction model is based on a combination of three types of friction Stribeck, Coulomb and viscous as shown in Figure 4-7.

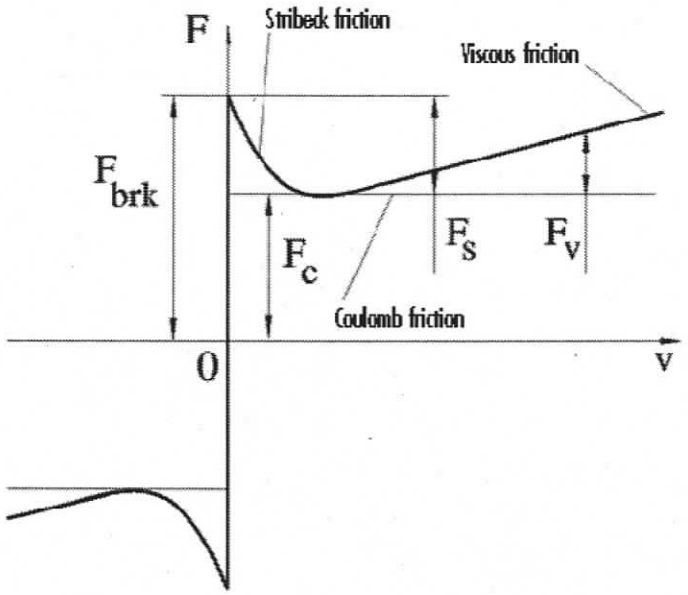

Figure 4-7: Transitional friction model [19].

It can be seen that Stribeck friction results in negatively sloped force curve at low velocities, coulomb friction results in a constant force independent of velocity and viscous friction produces an increasing force proportional to velocity. When velocity is zero, a force known as the breakaway force is required to allow the components to begin motion. The force of friction F_{fl} is described by equation 4.6 [19].

$$F_{fl} = (F_C + (F_{brk} - F_C)\exp(-c_v|v|)sign(v) + f_v \qquad \textbf{(4.6)}$$

The implementation of Equation 4.6 in Simulink presents a problem because of the discontinuity when velocity equals zero, and so equation 4.6 must be modified according to Figure 4-8 , as shown by equation 4.7-4.8 and as used in [19].

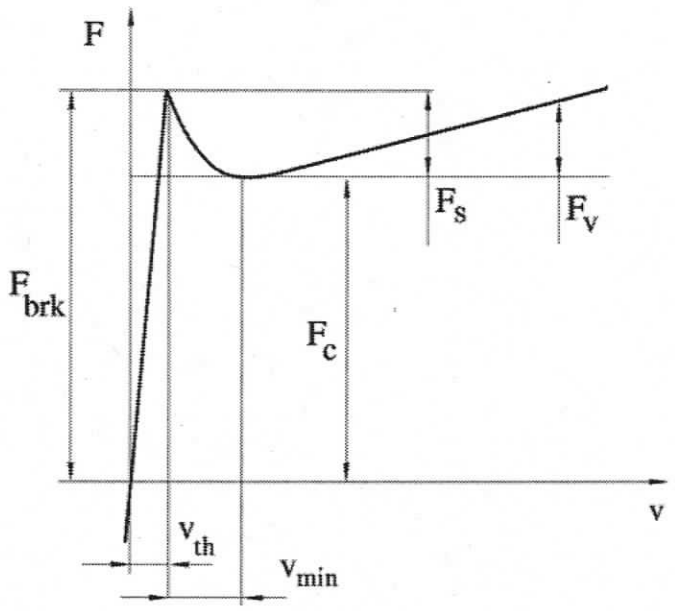

Figure 4-8: Modified friction model [19].

$$If|v| >= v_{th}$$
$$F_{fl} = (F_C + (F_{brk} - F_C)\exp(-c_v|v|)sign(v) + f_v \quad \textbf{(4.7)}$$

$$If|v| < v_{th}$$
$$F_{fl} = v\frac{(fv_{th} + (F_C + (F_{brk} - F_C)\exp(-c_v v_{th})))}{v_{th}} \quad \textbf{(4.8)}$$

The application of the model described by equation 4.7, 4.8 is difficult as the parameters are not always known. The Coulombic force F_C can be calculated using equation 4.9 where F_N is the normal force being applied by the tension O-ring. The normal force can be estimated from O-ring compression graphs as shown by Figure 4-9. The friction coefficient can be determined using standard tables.

$$F_C = \mu F_N \quad \textbf{(4.9)}$$

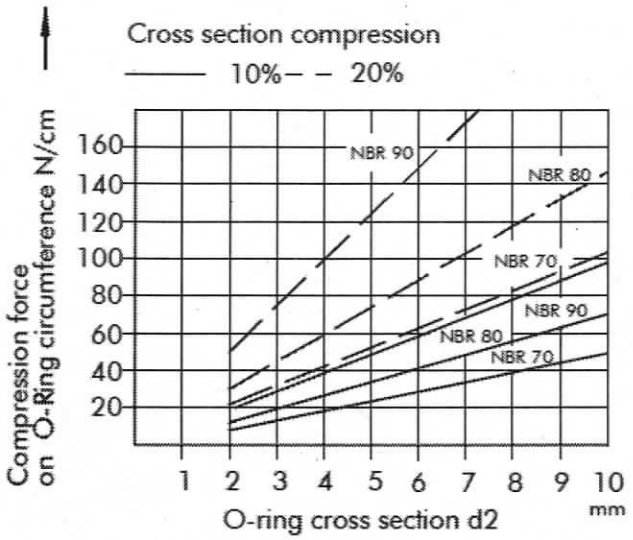

Figure 4-9: O-ring compression forces [22].

The breakaway friction F_{brk} is difficult to determine without sensitive measuring equipment. For the purpose of the injector model development, the break away friction force was estimated based on simple force measurements and then adjusted by fitting the motion model solution to a known lift measurement. The same procedure was used to determine the remaining parameters, such as viscous damping coefficient, as these values are heavily dependant on the application. The adjustment of these parameters was done by comparing the dynamic response of the model to a known lift profile. The breakaway force was adjusted by comparing the phase shift between the two profiles, whilst the damping coefficient was adjusted by comparing the dynamic response of the closing impact between needle and seat. Once the friction parameters have been determined, the friction model of the guide can be applied to other models assuming the guide geometry remains the same.

Table 4-2: Transition friction model parameters

Variable	Description	Value
F_{brk}	Guide break-away force	25 N
c_v	Transition approximation coefficient	5 s/m
f_v	Viscous friction coefficient	100 N s/m

v_{th}	Velocity threshold	0.0001 m/s
μ	Coulomb friction coefficient	0.05
F_N	Normal Force	15 N

4.2.4 Injector Pressure Model

Equation 4.1 contains a force term which describes the fuel pressure acting on the sealing surfaces of the injector needle. In a static state, the force can be calculated using equation 4.10 where P_i-P_o is the pressure difference between the internal injector pressure and the pressure just passed the injector seat. A_e is the area in which the pressure acts upon the needle.

$$F_P = (P_i - P_o)A_e \tag{4.10}$$

The development of a pressure model for the dynamic case (i.e. the injector is opening or closing) is a complex fluid dynamics problem. Hong [20] used Equation 4.10 to approximate the pressure difference. Their model involved calculating the area on which the pressure acts of a conical needle as the injector was opened or closed. The needle geometry is shown in Figure 4-10 (A). The determination of the downstream pressure was done experimentally.

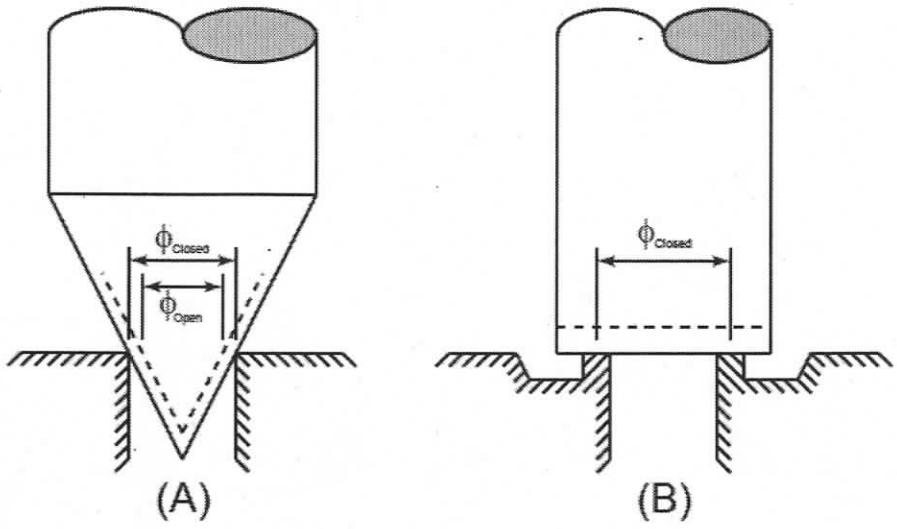

Figure 4-10: Effective opening areas injector needle designs.

Figure 4-10 (B) shows the typical seat design of a DA injector and it can be seen that in the closed position, the area which the pressure acts is given by the middle diameter of the sealing lips. When the injector is opened, there is no longer a surface on which the pressure acts, and so the force due to the fuel pressure becomes zero. As the injector begins to open (injector lift very small), the pressure difference before and after the seat is large and so a pressure force still acts. However, it can be said that the pressure force drops exponentially with increasing gap, which allows the pressure force to be neglected when the needle is not in contact with the seat. For the model developed in this thesis, equation 4.11 was used to approximate the effect of pressure on the needle.

$$\begin{aligned} &\text{if } x_2 \le 0 \\ &F_P = (P_i - P_o)A_e \\ &\text{if } x_2 > 0 \\ &F_P = 0 \end{aligned} \tag{4.11}$$

4.3 Injector Lift Measurement

In order to verify the injector model, actual lift measurements are used. This type of measurement can be taken by one of two methods: external accelerometer measurements or internal eddy current/capacitive lift sensors.

Figure 4-11 shows a sample of an accelerometer measurement performed on a DA fuel injector. The two solenoid current signals have been overlaid to help visualize the timing. The accelerometer signal shows two distinct points which indicate the impact of the injector needle with the stop and then the seat respectively.

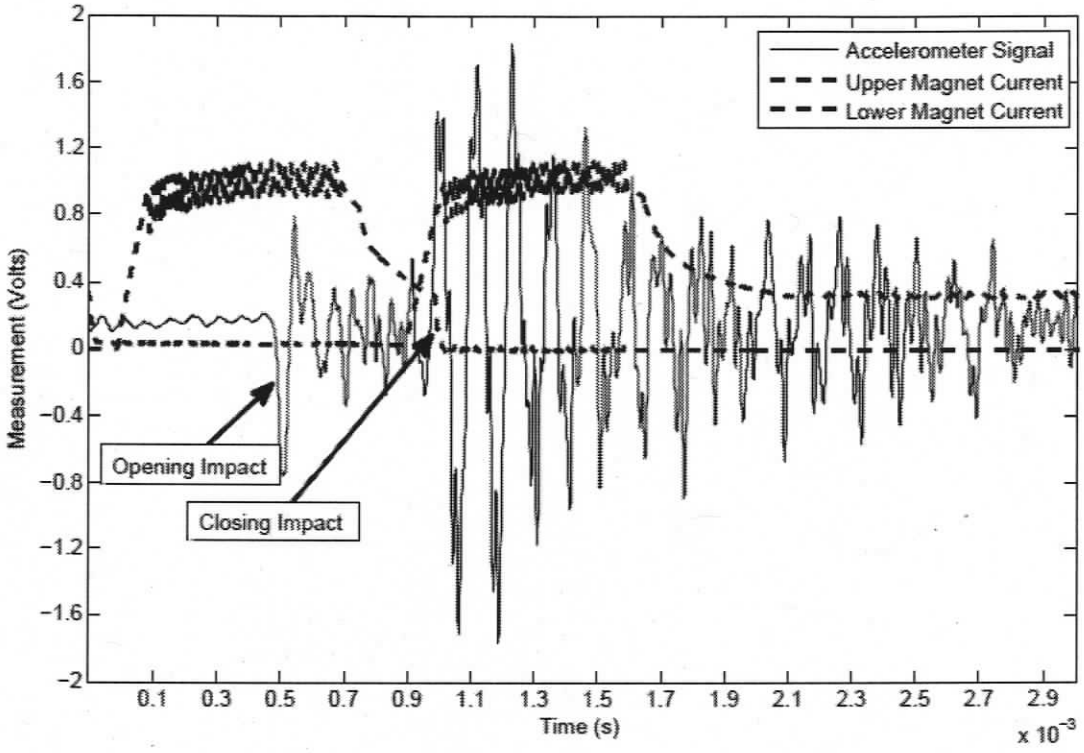

Figure 4-11: Sample accelerometer measurement.

The amount of information which can be recovered from a signal, such as the one shown in Figure 4-11, is limited to the time of impact. Information about maximum lift and shape of the lift profile cannot be determined; however, these are interesting parameters which can help to calculate impact forces as well as friction behaviour of injectors. To solve this problem, injectors can be fitted with internal lift sensors which are integrated into the components. The main problem encountered is the sealing of the sensors since they are small. The size and measurement accuracy of such sensors makes them expensive and hence, only suitable for laboratory experiments. The results of the lift simulation model have been compared to experimental measurements performed with an

integrated sensor as shown in Figure 4-12

4.4 Results of Injector Lift Model

The coupled second order differential equations describing the injector dynamics (Equations 4.1 and 4.2) are solved using the Matlab toolbox Simulink. The complete Matlab Simulink program tree is presented in Appendix C.

Figure 4-12 shows simulation results for a double acting high pressure injector. The results have been compared to lift measurements preformed with an eddy current type sensor installed within the gas connection of the injector. The overall agreement between measured and simulated is good, but it can be seen that the opening and closing profiles of the simulated injector react faster than the actual injector. The difference between the curves could be a result of a delay in the magnetic field due to eddy current losses in the solenoid. These eddy current losses are not modelled in the simulation as the force data used describes the maximum force for a static current. To verify this result, a dynamic simulation of the solenoid is required which is not within the scope of this thesis.

It can also be seen from Figure 4-12 that the slope of the closing profile is larger than the simulated profile. It is likely that this is due to the additional drag on the injector components, as the gas is flowing through and around them. As discussed in previous sections, the drag on the components was neglected in the model. The simulated and measured lift profiles show agreement in the amount of displacement on impact with the stop and seat, which indicates that the velocities at impact are similar and that the stop and seat spring and damping constants are correct.

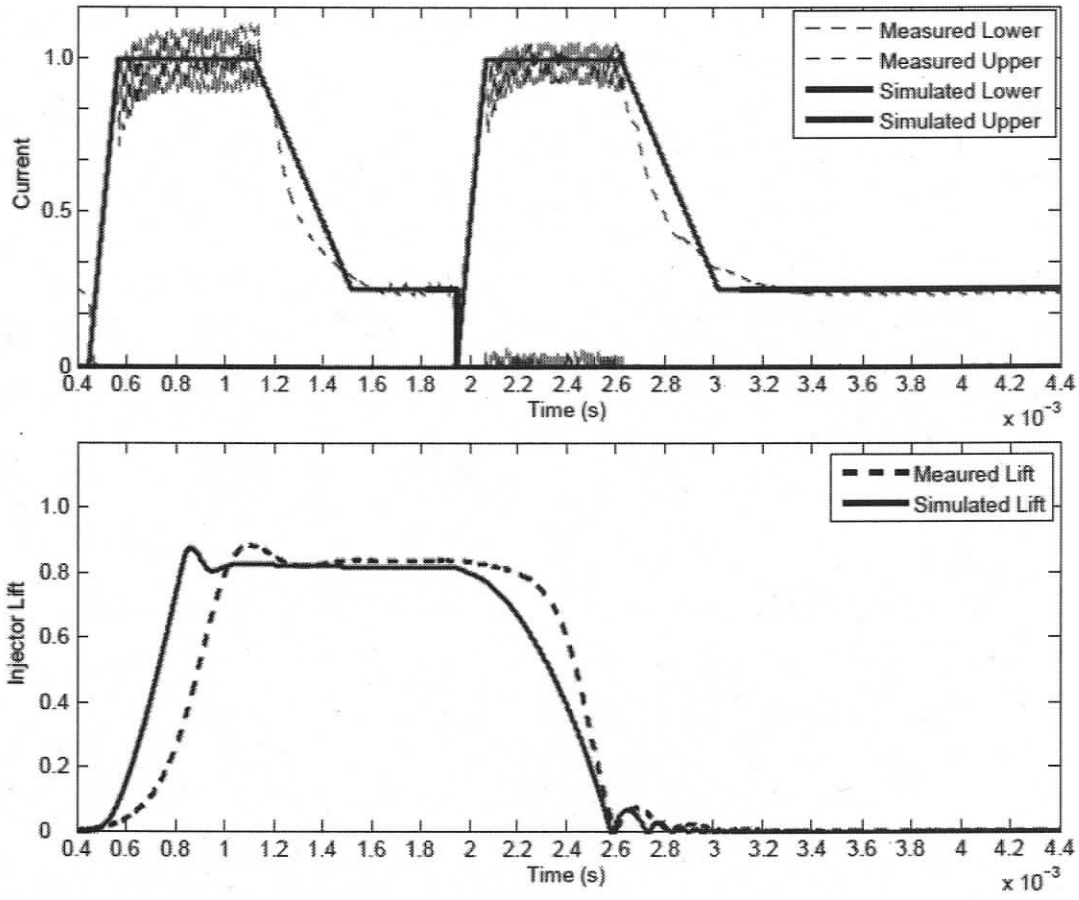

Figure 4-12: Results of lift model for high pressure DAI.

An important goal of the model was to simulate the impact forces on the seat and stop. Calculated forces are shown in Figure 4-13 and Figure 4-14. Figure 4-13 shows the forces acting on the stop while the needle is in contact. From the diagram it can be seen that the plastics material dissipates the impact energy quickly. The force after the initial impact is the force of the solenoid pulling the needle against the stop.

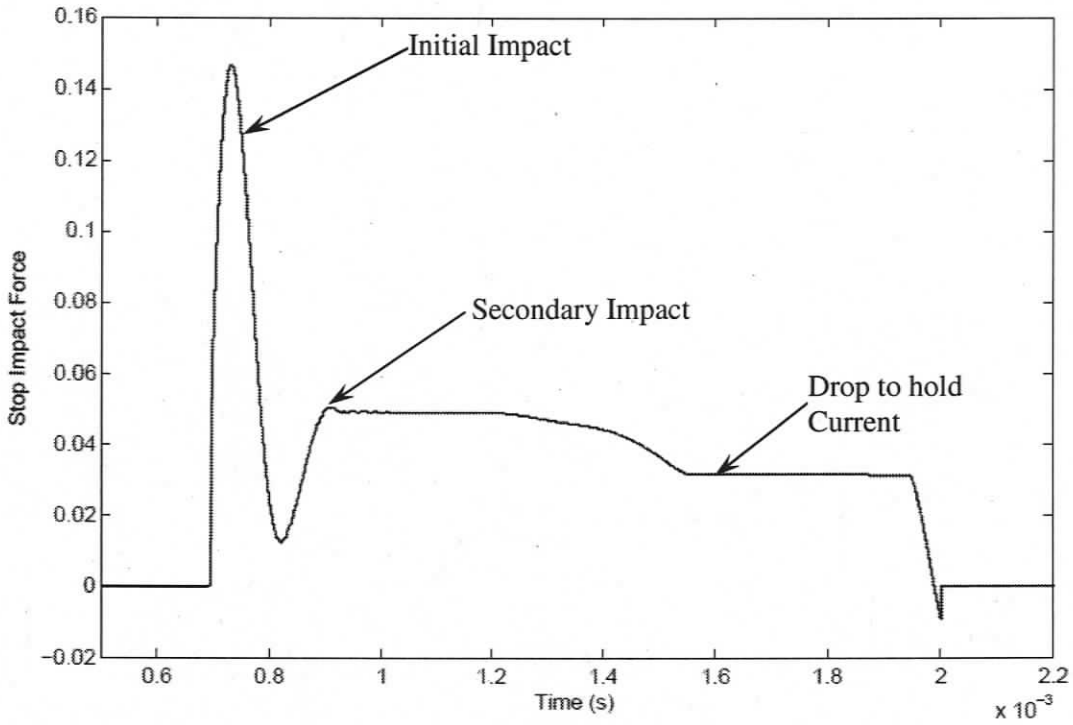

Figure 4-13: Stop reaction forces

Figure 4-14 shows the impact of the needle on the seat when the injector is closed. As can be seen, there is a series of impacts as the needle bounces off the seat. Because both components are steel, there is little-to-no damping which produces large force spikes. These force spikes are the main source of seat wear and must be kept at acceptable levels (defined by the seat coating allowable stress), or the design must incorporate some type of seat damping design; otherwise the seat will fail rapidly.

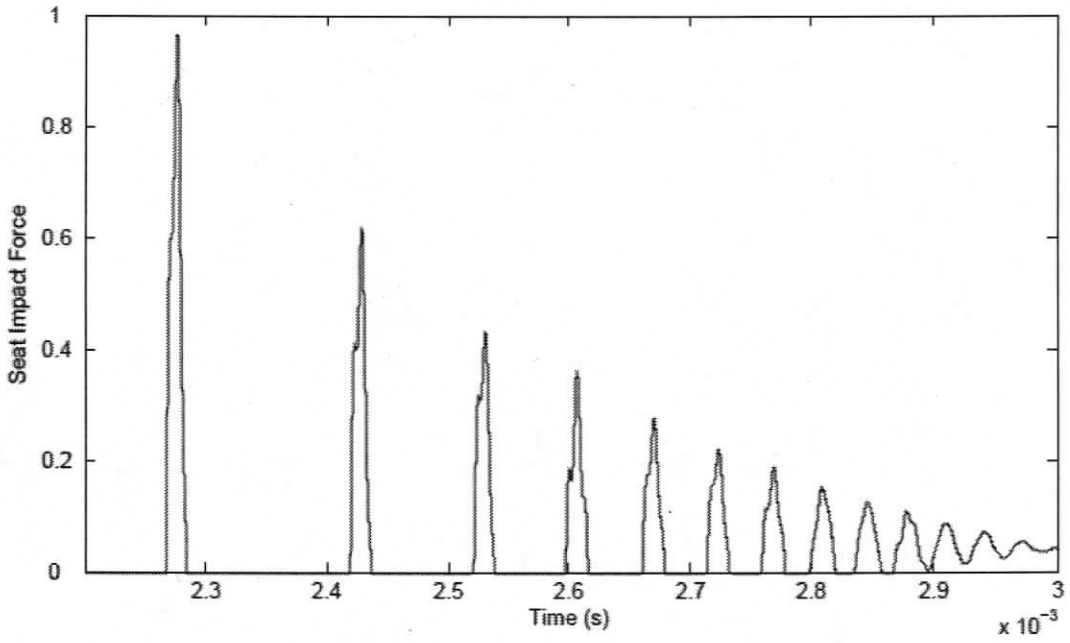

Figure 4-14: Seat reaction forces.

4.5 Optimization of Injector Performance

One objective of this thesis is to provide a method for optimizing the DA technology in terms of solenoid performance and cost. Chapter 3 showed that materials such as FeSi3% have comparable performance when compared to the current solenoid armature material combination at a fraction of the cost. Using the model developed above, it is possible to simulate the performance of a DA injector for the purpose of comparing dynamic injector response based on solenoid material. Figure 4-15 shows the results of such a comparison for a DA high pressure injector (100 bar). The figure shows that a FeCo17% Mat 2 solenoid provides the quickest response while, as expected, the tool steel reacts the slowest. The simulation shows only a slight deviation between the remaining materials which indicate that a solenoid manufactured from FeSi3% or FeSi1% would provide similar injector performance at much lower production cost then FeCo17% Mat 1. If cost is not considered and the injector concept focuses on performance, obviously FeCo17% Mat 2 is the material of choice.

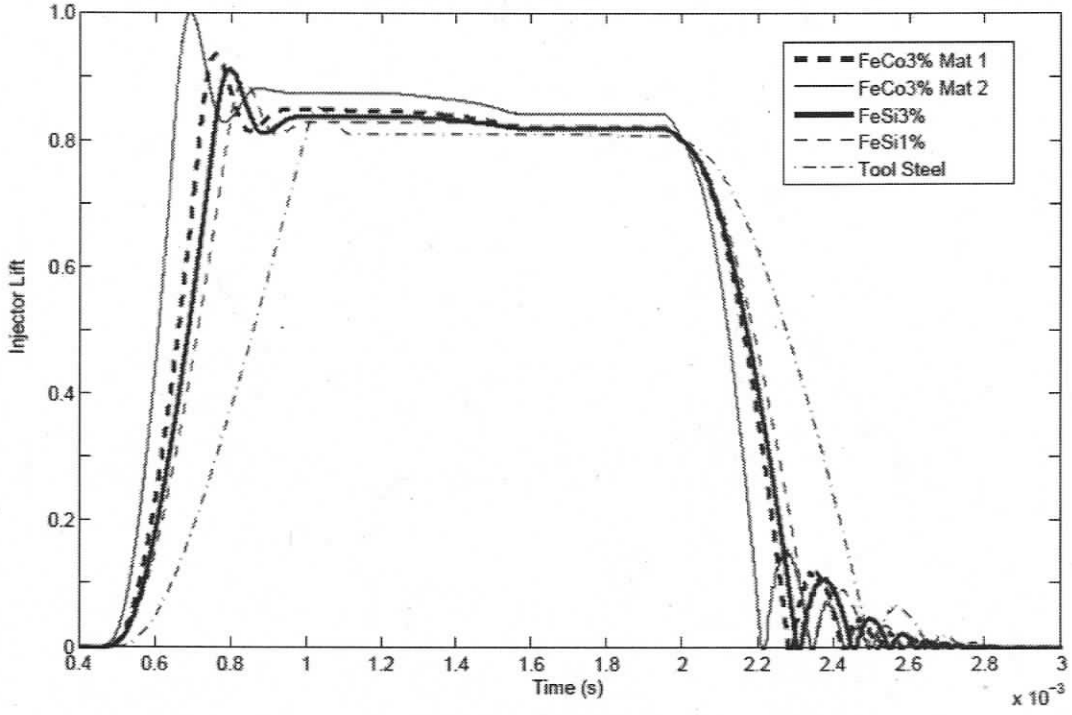

Figure 4-15: Simulated injector lift profiles for various solenoid materials

4.6 DA Seat Impact Force Reduction

Premature seat wear due to high impact stresses is one of the leading causes of failure for gaseous fuel injectors due to the lack of viscous damping which protects liquid injector seats. Due the high closing speeds which characterize DA injectors the seats used must be carefully designed to withstand the impact stress over the life of the injector. Using the dynamic lift model developed in previous sections different methods reducing the seat impact stresses will be investigated. The results shown will be compared to the standard configuration used to develop the model (i.e. steel seat, needle, and connecting rod).

4.6.1 Method 1: Modification of Seat Material

The simplest method, from a design point of view, to reduce impact forces between two components is to modify the material combination. Inclusion of a material which dissipates impact energy quickly such as a polymer can drastically reduce the impact forces as well the needle bounce. Figure 4-16 shows the needle lift and seat impact forces

where the model parameters have been modified according to Table 4-3 which represents a seat manufactured out of glass fibre reinforced polymer.

Table 4-3: Polymer Seat Model Parameters

Variable	Description	Value
k_p	Seat spring constant	6.25×10^7 N/m
d_p	Seat damping coefficient	200 N-s/m

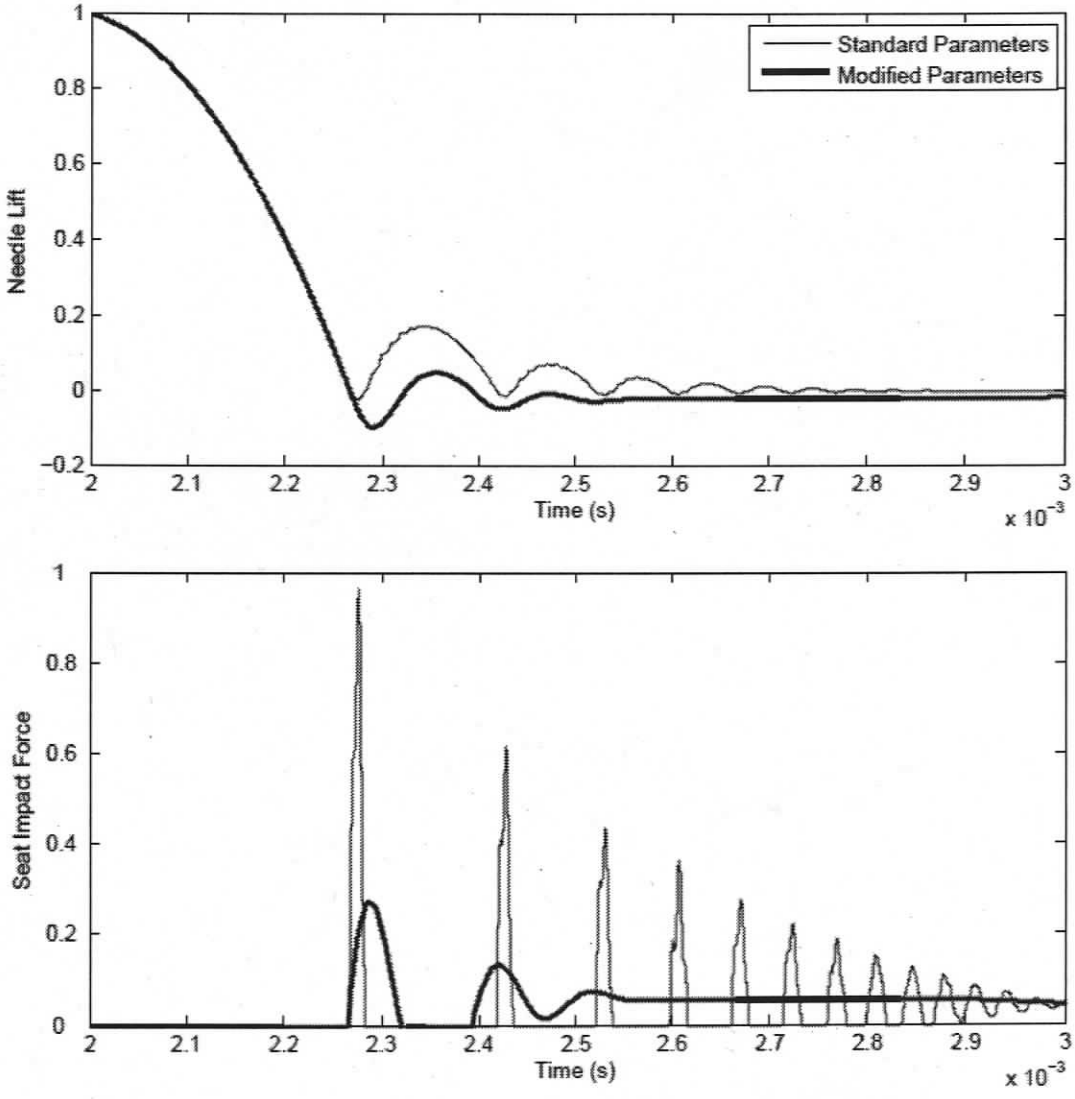

Figure 4-16: Polymer seat impact forces

From the lift profile it can be seen that the polymer material dissipates the impact energy quickly through elastic deformation which also reduces the needle bounce amplitude. The lift profile shows that care must be taken when designing polymer seats. The elastic deformation caused by initial impact should not be larger than the minimum require air gap otherwise impact between armature and solenoid will occur which must be avoided to guarantee long service life. The impact forces also show the advantage of a polymer seat which is represented by a reduction of the initial impact force of 67%. This drastically improves service life of seats as long as temperature is tightly controlled. Polymer materials for engine applications must retain there mechanical properties at elevated engine temperatures. By either choosing materials which have good high temperature characteristics or by making design choices which allow good temperature control such as cooling channel placement a polymer seat is a viable solution for improving DA injector seat life.

A second option in regards the seat is to spring load a steel seat which would produce a similar lift and force profile as shown in Figure 4-16 if a spring constant and damping coefficient similar to that of the polymer material is applied. The problem that arises is that options for such spring elements are limited. If temperature is an issue spring loading the seat with a polymer ring is not an option and alternative materials such as aluminium is considered too soft for such an application. The only other component known to the author which could fulfill these requirements is a steel disk spring. This is however also problematic due to limited space available under the seat.

4.6.2 Method 2: Modification of Connecting Rod Material

The use of alternative materials for the connecting rod between needle and armature was used by H.Hong et.al. [10 -12] to control needle bouncing for there single acting gaseous fuel injector design. The model of the DA injector was modified according to Table 4-4 to simulate an injector where the connecting rod is manufactured out of a glass reinforced polymer. Due to lower mass of the connecting rod the lumped masses m_1 and m_2 where also reduced accordingly.

Table 4-4: Polymer Rod Model Parameters

Variable	Description	Value
m_1	Armature mass	0.010798 kg
m_2	Needle mass	0.00254 kg
d_r	Connecting rod damping coefficient	200 N-s/m
k_r	Connecting rod spring constant	10.7×10^6 N/m

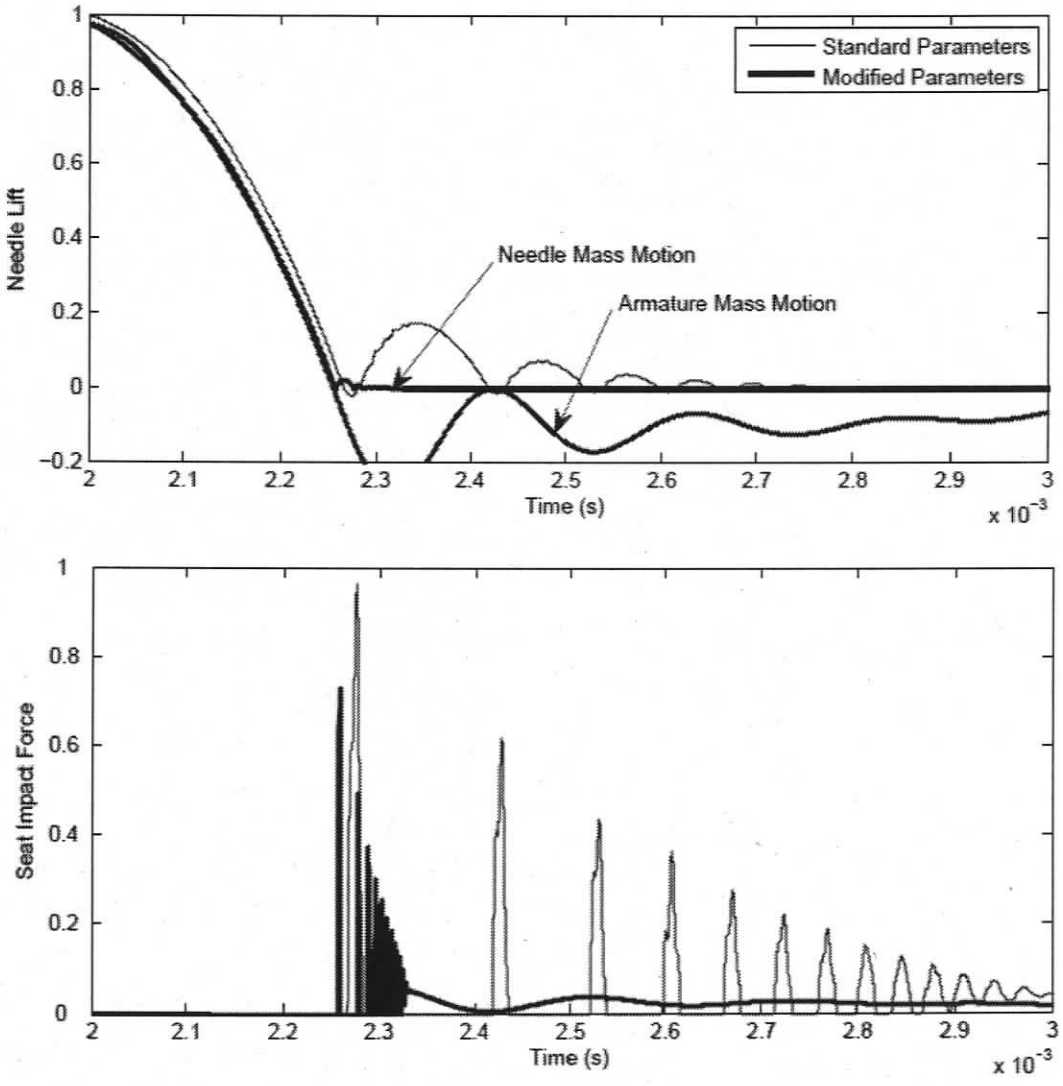

Figure 4-17: Polymer connecting rod impact forces

Figure 4-17 shows the resultant simulated lift profile and seat impact forces of a DA injector with a modified connecting rod as compared to the original design. The lift profile shows two advantages. The first is that due to reduced moving mass the reaction time of the injector has been reduced and second is that bouncing has nearly been eliminated. The force profile however only show a slight reduction in impact forces of about 25%. The reason for this is that the impact energy of the needle has not been reduced as there are no components which dissipate energy on impact. The resultant impact force of sub-sequent impacts are however reduced as the polymer rod damps the energy of the larger armature mass as shown by the second lift profile. The disadvantage is that the free motion of the armature might result in an impact with the solenoid if the geometric and material parameters of the connecting rod are not correctly chosen. The advantage of this method is that the polymer is not exposed to combustion temperatures as the fuel flow maintains a constant temperature. The problem that arises is one of thermal expansion due to the long shape factor of the connecting rod the polymer material must have a thermal expansion coefficient similar to that of steel if the fuel flow rate is to be constant over the normal operating range of an engine.

4.6.3 Method 3: Magnetic Braking

The final method of reducing impact forces involves keeping the original injector components and using an advanced control system to produce a magnetic brake. The idea behind the magnetic brake is to reduce the speed of the needle shortly before it impacts the seat reducing both bouncing and impact forces. Figure 4-18 shows what can be achieved using magnetic braking. When the upper solenoid hold current drops to zero the lower solenoid begins to pull the needle closed. When the control system which measures lift in real-time determines that the needle is a predetermined distance from the seat the controller applies a short burst of current to the upper solenoid which slows the needle. From the seat impact force it can be seen that the initial impact can be reduced by 65% which is comparable to the results of the polymer seat concepts with the added advantage a heat resistant design. The disadvantage of this method is however the precise control required and the need for an integrate lift sensor.

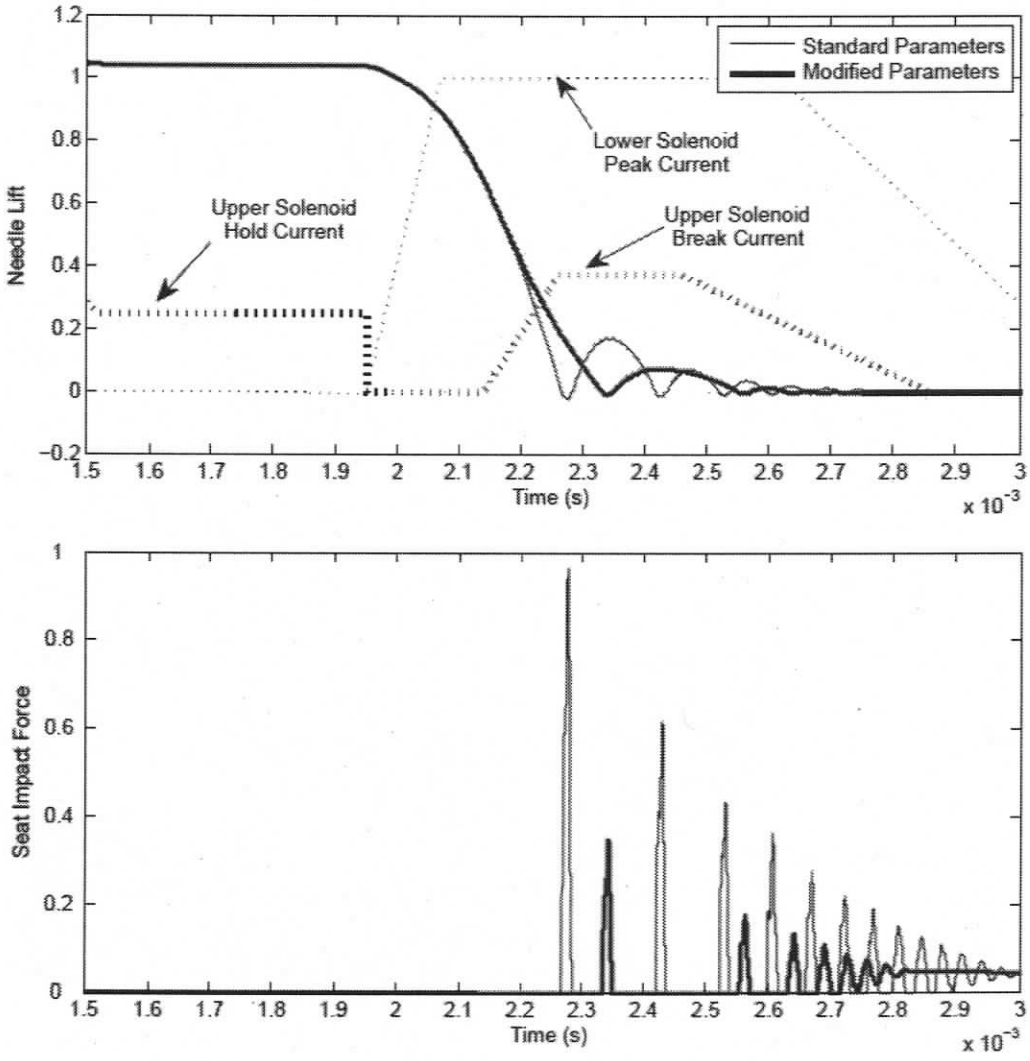

Figure 4-18: Results of magnetic breaking

4.7 Summary

Chapter 4 outlines the development of a dynamic lift model for DA injectors which predicts the motion of the injector needle. The model is developed using a second order mass, spring, damper system from which the equations of motion for each mass can be derived. Using Matlab Simulink these equation where transformed into a parameterized model which predicts motion of the needle and seat/stop impact forces. Using the model the performance of the various materials selected in Chapter 3 was computed for a high

pressure DA injector application. The model can also be used to optimize the shape and material of the both the seat and stop with the goal of reducing wear which leads to failure of the injector due the internal leakage. Three methods of seat impact damping where investigate, the results showed that a polymer seat or magnetic braking allow for significant reductions in impact forces while a polymer connecting rod between the two mass showed significant reductions in seat impact forces but also due the high momentum of the armature mass impacts between the armature and lower solenoid occurred.

Chapter 5 Conclusion and Recommendations

The objective of this thesis work was to develop analytical tools which can be used to optimize DA hydrogen fuel injectors in preparation for series production. The tools developed included a magnetic finite element model of the solenoid used to actuate the fuel injector and a dynamic response lift model. These models were developed to allow engineers to optimize the injector design in regards to material and manufacturing costs, performance and sealing/stop surface wear.

Using the current core design, the solenoid model was verified by comparing simulated results with actual measured values obtained using a specially designed test rig. The model was used to qualify further magnetic materials, including iron cobalt and iron silicon alloys, by comparing simulated and measured forces in order to verify the permeability models. The results can be used to optimize the selection process of solenoid materials based on performance and cost. Another advantage of the model is that alternative core geometries can be computed allowing geometric optimization of cores based on the customer requirements. It has been shown, that when the results from the model are compared to actual measured data they agree to within ±5% except in cases where material heat treatment is a significant factor on the materials magnetic properties.

One of the major problems faced by DA injector technology is the ability to control wear on the seat sealing surfaces and needle stop caused by the needle impact forces. The proper design and sizing of impacted components as well as material selection is an important means of reducing the wear on critical surfaces. The model developed in this thesis allows engineers to input material properties as well as component geometry to predict the injector motion under varying pressure and electrical conditions. It has been shown that this model predicts the injector motion with reasonable accuracy, although it has also been shown that electromagnetic dynamics play an important role in the initial opening and closing phases of motion as well as gas drag on flow geometry. Using the model three different methods of reducing the impact forces on the seat where tested. It was shown the largest reduction can be achieved by using seat materials which dissipate

impact energy by means of elastic deformation. A new concept of magnetic breaking also shows promise if a control system can be developed which meets the requirements and is also cheaply available for automotive applications.

Future work in the area of solenoid modeling should include a detailed study into the affect of heat treatment on the various magnetic materials with the goal of determining whether inexpensive heat treatments can increase the magnetic material force potential. Work should also be conducted in this area to further reduce core manufacturing costs through the application of new manufacturing processes like sintering or the application of new state of the art materials. The dynamic motion model should incorporate the results of a three dimensional dynamic solenoid model, taking into account the magnetic losses due to eddy currents. This should provide better accuracy of the lift model, as well as providing engineers with a method for optimizing magnetic cores to reduce dynamic loses which in turn would improve dynamic response of the DA technology. The lift model should also investigate the effect of gas flow on the movable components. A possible modeling system would involve the linking of the Simulink model developed here with a Comsol model which dynamically computes the magnetic forces.

Bibliography

[1] "December 2007 Dashboard", Hybridcars.com, January 25, 2008 <http://www.hybridcars.com/market-dashboard/dec07-overview.html>

[2] Robert Rose, "Fuel Cells and Hydrogen: The Path Forward", Fuelcells.org, January 2003, <http://www.fuelcells.org/info/pathforward.pdf>

[3] "AUTOMOTIVE MARKET – Application Overview", Ballard.com, http://www.ballard.com/Automotive_Fuel_Cells/Application_Overview.htm

[4] Basshuysen, Richard van, and Fred Schäfer. *Handbuch Verbrennungsmotor: Grundlagen, Komponenten, Systeme, Perspektiven*. Wiesbaden: Vieweg, 2005.

[5] Jiles, David, *Introduction to Magnetism and Magnetic Materials*. London: Chapman and Hall, 1991.

[6] J. Fidler and R. Grossinger, *Lecture Notes: Physics or Materials*. TU-Wien. VO 133 019. 2007

[7] James W. Heffel, Micheal N. McClanahan and Joseph M. Norbeck, *Electronic Fuel Injection for Hydrogen Fueled Internal Combustion Engines*, Society of Automotive Engineers International, Technical Paper # 981924, 1998

[8] Daniel M. Kabat and James W. Heffel, *Durability implications of neat hydrogen under sonic flow conditions on pulse-width modulated injectors*, International Journal of Hydrogen Energy Volume 27, Issue 10, October 2002, Pages 1093-1102.

[9] James Harrington et al., *Direct Injection of Natural Gas in a Heavy-Duty Diesel*

Engine, Society of Automotive Engineers International, Technical Paper # 2002-01-1630, 2002

[10] H.Hong, T. Krepec, and R. M. H. Cheng, *Optimization of Electronically Controlled Injectors for Direct Injection of Natural Gas Diesel Engines*, Society of Automotive Engineers International, Technical Paper # 930928, 1993

[11] Harry Kekedjian and Tadeusz Krepec, *Further Development of Solenoid Operated Gas Injectors with Fast Opening and Closing*, Society of Automotive Engineers International, Technical Paper # 940450, 1994

[12] Henry Hong, *Optimum Performance of Solenoid Injectors for Direct Injection of Gaseous Fuels in IC Engines*, PHd Dissertation Concordia University, Montreal, Canada, 1995

[13] F.Meier, J. Koehler, W. Stolz, and W. H. Bloss, *Cycle-Resloved Hydrogen Flame Speed Measurement with High Speed Schlieren Technique in Hydrogen Direct Injection SI Engine*, Society of Automotive Engineers International, Technical Paper #942036, 1994

[14] C. J. Rallis, S. A. Habbitts and R. van Dijk, *A hydraulically controlled diaphragm-type hydrogen gas injector*, International Journal of Hydrogen Energy Volume 22, Issues 10-11, October-November 1997, Pages 1071-1073.

[15] Kistler Instrument Corp, *Quarz-Kraftmesselmente datasheet*, kistler.com, Document reference: 000-107m-12.96 (DB06.013m-12.96)

[16] Comsol Support, *Introduction to AC/DC Module*, Comsol.com, http://www.comsol.com/products/acdc/

[17] Walther-Meißner-Institute, *SQUID Magnetometry*, wmi.bad.de, 2007,

<http://www.wmi.badw.de/methods/squid.htm>

[18] B. Armstrong, C.C. de Wit, *Friction Modeling and Compensation*, The Control Handbook, CRC Press, 1995

[19] Matlab Simscape Documentation, *Transitional Friction*, mathworks.co.uk, http://www.mathworks.co.uk/access/helpdesk/help/toolbox/physmod/hydro/ref/cylinderfriction.html

[20] H. Hong and B Torab, *Solenoid-operated diesel injectors for low-viscosity liquid and gaseous fuels*, Journal of Automobile Engineering, Volume 215 Part D, 2001

[21] Jochen Pohl, Magnus Sethson, Petter Krus and Jan-Ove Palmberg, *Modelling and Simulation of a Fast 2/2 Switching Valve*, Linkoeping University, Sweden

[22] Trelleborg, *O-ring Handbook*, tss.trelleborg.com, <http://tss.trelleborg.com/com/www/media/downloads/catalogs/o_ring_gb.pdf>

Appendix A – Magnetic Materials

Magnetic materials can be separated into two categories: soft and hard. A soft magnetic material has little remanence, while a hard magnetic material retains a net polarization after the removal of an applied field. Figure A-0-1 shows a table of common magnetic materials used in industrial applications subdivided into soft or hard.

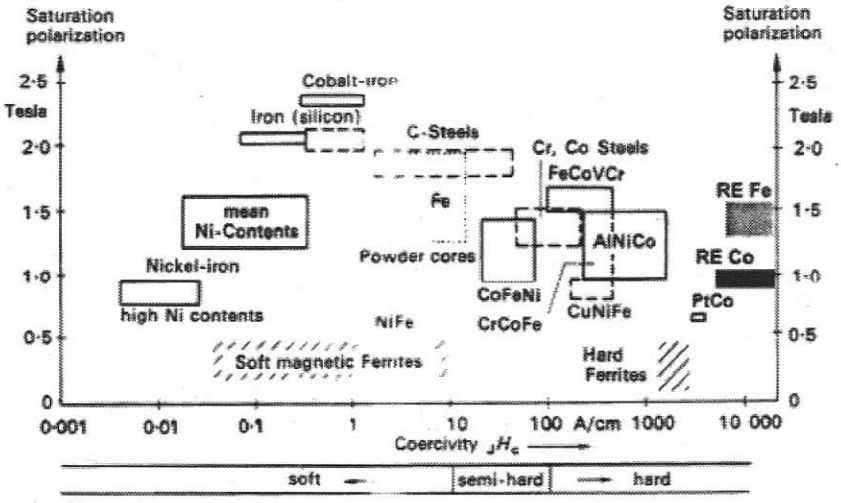

Figure A-0-1: Characterization of magnetic materials [6]

Permeability is an important parameter of ferromagnetic materials as it relates magnetic flux density to magnetic field strength. Another interpretation is how easily flux travels through a material. In soft magnetic materials, the differential permeability is not a constant value. Instead, it is defined as the ratio of flux density to magnetic field strength (*B-H* diagram) as shown in Figure A-0-2.

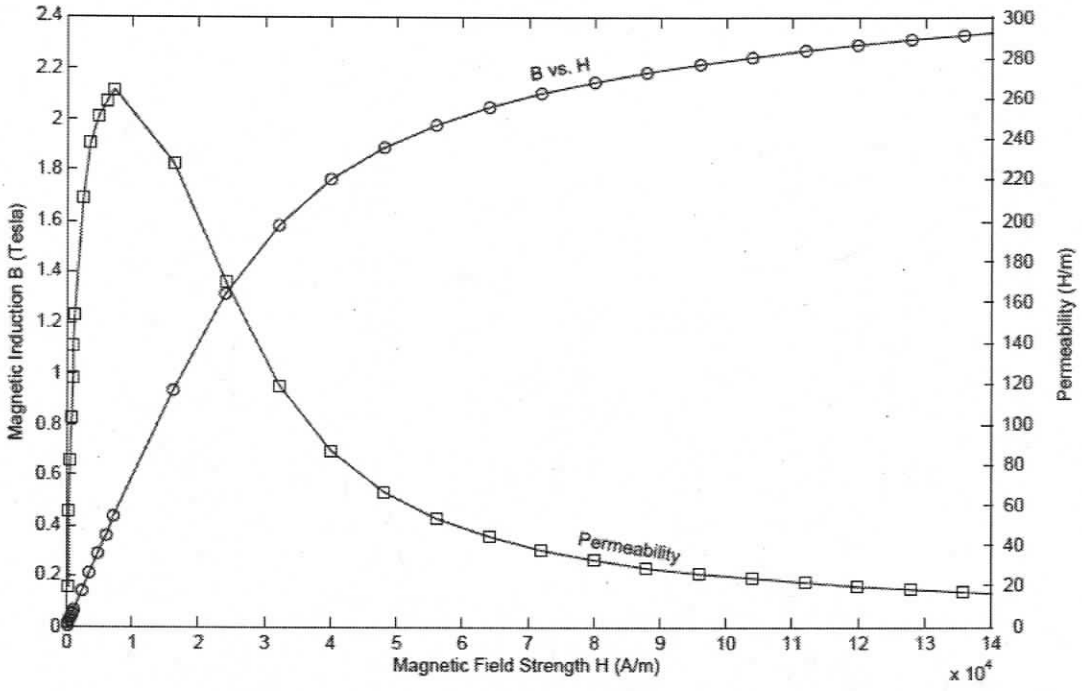

Figure A-0-2: Permeability of a B-H diagram

Figure A-0-3 shows a complete B-H diagram of a magnetic material over a range of magnetic field strengths. The B-H diagram shows that the material has hysteresis. The dotted line represents the initial material state under initial magnetization. The hysteresis is then caused by remnant magnetization in the material. The B-H diagram also shows that there is a limit to the magnet field, as the field strength increases magnetic domains align with the field until nearly all domains are aligned. At this point any further energy applied into the material is converted to heat. This point is known as the saturation magnetization and is shown as the flatting at the end of the B-H diagram. Remanence is defined as the amount of magnetization which remains within a material. The remanence of a material is the parameter which defines the hysteresis loop. If the remanence is high, the area bound by the loop is large and the remaining magnetic field is large. Magnetic materials used for solenoids show little to no remanence, as this could lead to a situation where the armature and core stick together and retard the injector's ability to close.

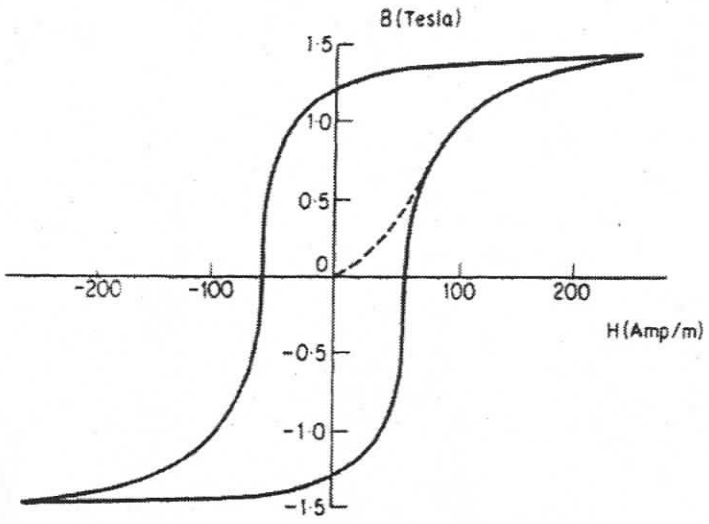

Figure A-0-3: Example magnetic material hysteresis curve [8]

Iron Cobalt Alloy

Iron cobalt is currently the material of choice for DA solenoids since it has good, soft magnetic properties, but it also has poor manufacturing properties. FeCo50% is an alloy which has good magnetic properties due to its 50-50 ratio of iron and cobalt. However, the high cobalt content makes the material difficult to machine since it has a high tool wear rate and it smears, which makes tight tolerance unreachable. The high cobalt content also comes at a high price—per tonne it costs 2 – 3 times more than its competing alloys FeCo17% Mat 1 and FeCo17% Mat 2. FeCo17% Mat 1 and FeCo17% Mat 2 are essentially the same materials, but manufactured by two competing companies. Both materials contain 17% cobalt, which gives good magnetic properties at reasonable cost. These materials have better machining properties, but are still considered critical compared to machining properties of tool steel. Iron cobalt alloys are highly susceptible to corrosion, so components must either be stored in moisture free environments or coated in oil. Once the injector goes into service, corrosion is typically not a problem, as the gaseous fuels are free of moisture.

Iron Silicon Alloy

Iron silicon alloys have an advantage over iron cobalt alloys since iron silicon has comparable magnetic properties but can be easily and cheaply obtained due to it's dominant market position in the transformer industry. The material costs 3 times less per tonne as iron cobalt and can normally be obtained in small amounts unlike iron cobalt where minimum tonnages apply. A further advantage of this material is that it has machining properties similar to that of normal tool steel, which makes complex core geometries cheaper to manufacture. Due to the addition of silicon, the material also has a good hardness of around 200HB. As with iron-cobalt alloys, this material is also highly susceptible to corrosion if stored in moist atmospheres and therefore must either be stored in dry conditions or coated in machine oil. The handling of these components can only be untaken with gloved hands, as the oils and salts on finger tips cause corrosion damage.

The material selected for comparison purposes is an iron silicon alloy which contains 3% silicon. In addition to the high silicon content material, another material FeSi1% will also be investigated. This material has an inclusion of 1.1% silicon, and so the magnetic performance should be lower when compared to the 3% alloy, but this material also contains 13.3% chromium and is classified as a stainless steel. This is a very rare combination of adequate magnetic properties and corrosion resistance and is interesting for gaseous fuel injection systems, which operate in the natural gas pipeline industry. FeSi1% also has the advantage that its price per tonne is comparable to that of standard tool steel and its machinability is similar to that of standard stainless steels

Tool Steel

This material is used for low end electromagnetic cores because it is cheap and readily available on the market. The material composition is not optimized for magnetic applications, but it has excellent machining properties which is an advantage in terms of cost when magnetic performance is not critical. This material will be considered the base line material which all the other materials are compared to in the further analysis.

Appendix B – Permeability using SQUID Magnetometry

SQUID stands for Superconducting Quantum Interference Device, and is one of the most effective and sensitive methods for measuring magnetic properties. This method has a distinct advantage in that it can directly determine the magnetic moment of a sample in absolute units. The instrument used to perform the measurements was a commercial SQUID magnetometer built by Quantum Designs. The sample is placed in a superconducting pick-up coil, as shown in Figure B-0-1, which pick-ups the magnetic signal of the sample.

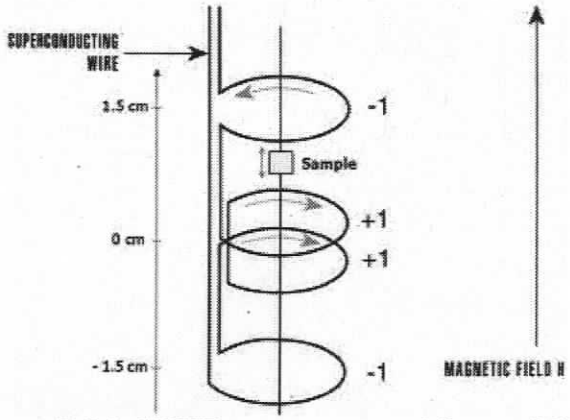

Figure B-0-1: SQUID magnetometer pick-up coil [17]

The coil and the SQUID antenna, as shown in Figure B-0-2, transfer the magnetic flux from the sample to an rf SQUID device which is separated from the sample by a liquid helium bath. This system acts as a flux to voltage converter where the signal, with the help of the magnetometer's electronics, is amplified and recorded. To begin measuring, the sample is moved up and down, thereby producing alternating magnetic flux in the pick-up coil, which in turn produces an alternating output voltage of the SQUID device. By linking the frequency of the read out to the frequency of the movement, the magnetometer system achieves a sensitivity of 10^{-11} Joules per Tesla which corresponds to the saturation magnetisation of an iron sample which has the size of six billionths of a cubic millimetre. To record a complete B-H diagram, the externally applied magnetic field shown in Figure B-0-1 is varied over the range of interest. As solenoid for injector application often enter the saturation region a field range of 2000Oe to -2000Oe were

swept starting at 2000Oe down to -2000Oe and then back to 2000Oe (2000Oe = 159863 A/m)

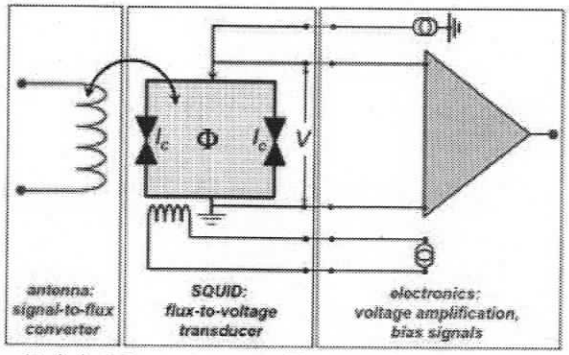

Figure B-0-2: Magnetometer flux to voltage converter [17]

The shape of the sample influences the measurement of the B-H curve due to demagnetizing fields. Demagnetizing fields are present in any magnetized material with finite dimensions. These fields are caused by the fact that the magnetisation and magnetic field point in opposite directions due to the dipole moment caused by the finite dimensions. Demagnetising fields are always present when magnetic dipoles are formed in a material and depend on two factors: magnetization in the material and sample shape. The Demagnetising field is given in equation B.1, where N_d is a factor calculated based on the geometry of the sample. Table B-1 shows a list of factors for different simple geometries.

$$H_d = N_d M \qquad \textbf{(B.1)}$$

Table B-1: Demagnetizing factors for various simple geometries [8]

Geometry		N_d
Toroid		0
Long cylinder		0
Cylinder	l/d = 20	0.00617
Cylinder	l/d = 10	0.0172
Cylinder	l/d = 8	0.02
Cylinder	l/d = 5	0.040
Cylinder	l/d = 1	0.27

Sphere	0.333

The demagnetising factor leads to errors during the measurement of a sample with finite length. The errors will increase as the length of the sample decreases. This effect is called shearing of the hysteresis loop and shows up as an elongation of the B-H loop along the H axis, which indicates a reduction in the material susceptibility. Therefore the magnetic field strength must be corrected using equation B.2

$$H_{in} = H_{app} - N_d M \qquad \textbf{(B.2)}$$

As described above, the sample geometry used to measure the B-H loop has a significant effect on the results. However, the samples are also further restricted by the limitations of the SQUID magnetometer machine. If a sample is too large, the magnetic moment becomes large and over-stresses the sample mounts, causing failure and possible damage to sensitive equipment. Samples are mounted into the SQUID Magnetometer and glued between two specially designed straws made of plastic to ensure no influence on the results. The samples measured were cylindrical and used the form factor of l/d = 10. Initial samples were manufactured to have a length of 10mm and diameter of 1 mm. Due to the large range of field (2000 Oe), these samples proved to be too large and the mounting straws broke, causing the sample to impact the field generating coil at high speed and resulting in damage and a week of downtime for the system. To solve the problem, the samples were reduced in size while still remaining within the l/d = 10 form factor. The sample dimensions are shown in Figure B-0-3.

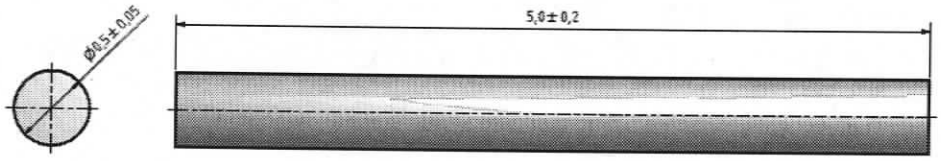

Figure B-0-3 : Sample Dimensions l/d = 10

The sample material structure is also an important factor, so each material was heat treated according to the applicable electromagnet core manufacturing guidelines eliminating any heat treatment effects.

The data obtained from the SQUID magnetometer measurement device is provide in typical units normally used by physicists as they describe the magnetization independent of volume. In many physics applications, a B-M (magnetization) loop is typically presented. For applications, engineers prefer B-H diagrams and standard metric units of (A/m). The data for field (H) was obtained in Oersted (Oe) and can be converted to field (H) in A/m by using equation B.6

$$H_{A/m} = H_{Oe}\frac{10^3}{4\pi} \qquad \textbf{(B.3)}$$

The data for magnetic moment was obtained in electromagnetic units (emu) and can be converted to magnetization in A/m using equation 2.7

$$M = \frac{Mo}{V}10^3 \qquad \textbf{(B.4)}$$

The field can now be corrected using the magnetization obtained from equation B.3 and equation B.4 using the correction $N_d = 0.0172$ from Table B-1. Magnetic induction (B) can now be calculated using equation B.5

$$B = \mu_o(H + M) \qquad \textbf{(B.5)}$$

Appendix C – Lift Simulation Simulink Program